manufacturer's instructions. For cytokine profiling of a HTLV-1–specific $CD4^+$ T cell line, cells were stimulated with formaldehyde-fixed ILT-#350 for 48 h. Culture supernatant was collected, and various cytokines were measured using a Human Th1/Th2/Th17 Cytokine Kit for a Cytokine Beads Array (BD Biosciences).

Induction of HTLV-1–specific $CD4^+$ T cell line (T4 cells)

PBMCs (1×10^6 cells/ml) from patient #350, in complete remission at 180 d after allo-HSCT, were cultured for 2 wk with 100 nM Tax301–309 peptide in 96-well round-bottom tissue culture plate (BD Biosciences) in a final volume of 200 μl RPMI 1640 medium with 20% FCS and 10 U/ml rhIL-2. $CD4^+$ cells were then isolated by negative selection using a Human CD4 T lymphocyte Enrichment Set-DM (BD Biosciences) and maintained in RPMI 1640 medium with 20% FCS and 100 U/ml rhIL-2. Cells (1×10^6 cells/ml) were stimulated with formaldehyde-fixed ILT-#350 (2.5×10^5 cells/ml) every 2–3 wk. After multiple rounds of stimulation, the resulting $CD4^+$ T cell line was assessed for HTLV-1 specificity by comparing IFN-γ production against ILT-#350 to that against an HTLV-1–negative cell line, LCL-#350.

RT-PCR

Total RNA from cells was isolated using Isogen (Nippon Gene, Tokyo, Japan) and Turbo DNA-free (Life Technologies). First-strand cDNA was prepared from 0.5 μg RNA using ReverTra Ace and $Oligo(dT)_{20}$ primers provided in a ReverTra Ace-α-kit (Toyobo, Osaka, Japan). PCRs were performed in 50 μl reaction mixture containing ReverTra Dash (Toyobo), 0.5 μM of each HTLV-1 pX-specific primer (pX1, 5′-CCA CTT CCC AGG GTT TAG ACA GAT CTT C-3′ and pX4, 5′-TTC CTT ATC CCT CGA CTC CCC TCC TTC CCC-3′), and 2 μl cDNA. GAPDH-specific primers (GAPDH5′, 5′-ACC ACA GTC CAT GCC ATC AC-3′; GAPDH3′, 5′-TCC ACC ACC CTG TTG CTG TA-3′) were used as an internal control. The thermal cycling conditions comprised an initial activation step at 94°C for 1 min, followed by 30 cycles of denaturation (98°C, 10 s), annealing (60°C, 2 s), and extension (74°C, 30 s). The PCR amplicons were visualized by ethidium bromide staining following 2% (w/v) agarose gel electrophoresis.

Flow cytometry

For cell surface staining, the following fluorochrome-conjugated mouse anti-human mAbs were used: CD3-FITC (UCHT1; BioLegend, San Diego, CA), CD4-FITC (RPA-T4; BioLegend), CD8-FITC (RPA-T8; BioLegend), and CD8-PE-Cy5 (HIT8a; BD Biosciences, San Jose, CA). For tetramer staining, PE-conjugated HLA-A*0201/Tax11–19, HLA-A*1101/Tax88–96, HLA-A*1101/Tax272–280, and HLA-A*2402/Tax301–309 tetramers were purchased from Medical & Biological Laboratories (Nagoya, Japan). PE-conjugated HLA-DRB1*0101/Tax155–167 tetramer were newly generated through the custom service of Medical & Biological Laboratories. Whole-blood or cultured cells were stained with PE-conjugated Tax/HLA tetramer in conjunction with CD3-FITC and CD8-PE-Cy5 or CD4-PE-Cy5. For whole-blood samples, RBCs were lysed and fixed in BD FACS lysing solution (BD Biosciences) before washing. Samples were analyzed on a FACSCalibur (BD Biosciences), and data analyses were performed using FlowJo software (Tree Star, Ashland, OR).

Epitope mapping

T4 cells (3×10^5 cells/ml) were stimulated with LCL-#350, pulsed with various concentrations of synthetic peptides for 1 h at 37°C, at a responder/stimulator (R/S) ratio of 3. The culture supernatant was collected at 6 h poststimulation, and peptide-specific IFN-γ production from T4 cells was determined by ELISA.

HLA class II restriction assay

T4 cells (5×10^5 cells/ml) were cocultured for 6 h with ILT-#350 (1×10^5 cells/ml) in the presence or absence of anti-human HLA-DR (10 μg/ml; L243; BioLegend), anti-human HLA-DQ (10 μg/ml; SPVL3; Beckman Coulter, Fullerton, CA), or anti–HLA-ABC (10 μg/ml; W6/32; BioLegend). The IFN-γ in the supernatant was measured by ELISA.

To identify a HLA class II molecule responsible for Ag presentation to T4 cells, Tax155–167 peptide-specific IFN-γ responses were evaluated using various HLA-typed LCLs (LCL-#350, LCL-#341, LCL-#307, and LCL-Kan). These LCLs (1×10^5 cells/ml) were pulsed with 100 ng/ml Tax155–167 peptide for 1 h, fixed with 2% formaldehyde, and then cultured with T4 cells (3×10^5 cells/ml) for 6 h. The culture supernatant was collected, and IFN-γ in the supernatant was measured by ELISA.

Tetramer-based proliferation assay

PBMCs (1.0×10^6 cells/ml) were cultured for 13 or 14 d with or without 100 nM antigenic peptides in the presence of 10 U/ml rhIL-2. Cells were stained with HLA/Tax tetramer-PE, CD3-FITC, and CD8-PE-Cy5 or CD4-PE-Cy5 and then analyzed by flow cytometry.

Statistic analysis

Statistical significance was evaluated with the unpaired t test using Graphpad Prism 5 (Graphpad Software, La Jolla, CA). In all cases, two-tailed p values <0.05 were considered significant.

Results

Tax-specific T cell responses in ATL patients who received allo-HSCT with RIC

We previously reported that Tax-specific $CD8^+$ T cells were induced in some ATL patients after allo-HSCT with RIC from HLA-identical sibling donors (10). In this study, we examined the Tax-specific T cell response in a larger number of ATL patients who received allo-HSCT with RIC. Table I provides a summary of the

Table I. Clinical information and summary for Tax-specific $CD8^+$ T cells in 18 ATL patients at 180 d post–allo-HSCT with RIC

ID (Age, Sex)	ATL Subtype	Type of Donor	Donor-HLA	Donor HTLV-1 Sero Status	Chimerism (%)[a]	Tetramer (%)[b]	Proviral Load[c]
239 (55, M)	Lymphoma	r-PB	A 26/33, DR 4/13	(−)	<5	NT	0.1
241 (61, F)	Acute	r-PB	A 2/26, DR 10/18	(−)	<5	0.00	0.1
247 (52, F)	Lymphoma	r-PB	A 24/−, DR 9/15	(−)	<5	0.07	0.1
270 (57, M)	Lymphoma	r-PB	A 24/33, DR 13/15	(−)	<5	0.00	0.0
300 (53, F)	Lymphoma	r-PB	A 24/26, DR 4/15	(+)	<5	1.34	4.8
301 (57, F)	Acute	ur-BM	A 24/33, DR 13/15	(−)	<5	0.72	0.0
307 (68, F)	Acute	r-PB	A 2/11, DR 14/15	(+)	<5	0.10	5.4
317 (60, M)	Acute	ur-BM	A 2/24, DR 14/15	(−)	<5	0.92	0.0
328 (62, M)	Acute	ur-BM	A 11/24, DR 8/9	(−)	<5	0.75	NT
340 (50, M)	Acute	r-PB	A 2/24, DR 4/8	(−)	<5	1.40	0.7
341 (61, F)	Acute	ur-BM	A 24/33, DR 1/15	(−)	<5	0.45	0.1
344 (58, M)	Lymphoma	ur-BM	A 2/24, DR 4/−	(−)	<5	0.44	0.0
349 (53, M)	Acute	r-PB	A 24/−, DR 8/15	(+)	<5	0.00	0.0
350 (60, F)	Acute	ur-BM	A 24/26, DR 1/14	(−)	<5	0.59	0.6
351 (57, F)	Acute	ur-BM	A 24/26, DR 9/12	(−)	<5	0.45	0.0
358 (63, F)	Lymphoma	r-PB	A 2/11, DR 4/14	(−)	<5	0.42	0.0
352 (61, M)	Acute	ur-BM	A 11/26, DR 8/15	(−)	<5	0.14	0.0
364 (52, M)	Acute	r-PB	A 24/26, DR 1/−	(−)	<5	0.11	0.0

[a]Indicates percentage of recipient-derived T cell chimerism.
[b]Indicates percentage of tetramer$^+$ cells among $CD8^+$ T cells in PBMCs.
[c]Indicates copy number per 1000 PBMCs.
F, Female; M, male; NT, not tested; r-PB, related donor-derived peripheral blood stem cell; ur-BM, unrelated donor-derived bone marrow cell.

results of Tax-specific $CD8^+$ T cell detection by flow cytometry, using the Tax/HLA tetramers, in the peripheral blood of 18 ATL patients at 180 d after allo-HSCT, together with clinical information. During this period, all patients achieved a complete chimera state consisting of >95% of donor-derived hematopoietic cells. By using four available tetramers (HLA-A*0201/Tax11–19, HLA-A*2402/Tax301–309, HLA-A*1101/Tax88–96, and HLA-A*1101/Tax272–280), Tax-specific $CD8^+$ T cells were found in 14 patients. Because the donors were uninfected individuals in the majority of cases (Table I), induction of the Tax-specific donor-derived $CD8^+$ T cells in recipients indicated the presence of newly occurring immune responses against HTLV-1 in the recipients. This evidence strengthens our previous observation (10, 32).

We also used a GST–Tax fusion protein-based assay to evaluate Tax-specific T cell responses. The tetramer-based assay was limited to four kinds of epitopes and restricted by three HLA alleles but did not detect T cells directed to other epitopes or HLAs. The GST–Tax fusion protein-based assay can detect both $CD4^+$ and $CD8^+$ T cell responses, irrespective of HLA types. However, this sensitivity is not as good as single-cell analysis by flow cytometry (31). As shown in Fig. 1A, there was a wide variation in the IFN-γ responses to the Tax protein in the PBMCs among the 16 patients tested. In five patients (#247, #270, #328, #340, and #349), IFN-γ production of PBMCs against GST–TaxABC proteins was very low or not specific for the Tax protein. PBMCs from the other 11 patients (#239, #241, #301, #317, #341, #344, #350, #351, #352, #358, and #364) produced higher amounts of IFN-γ in response to GST–TaxABC proteins compared with GST. However, the levels of IFN-γ production varied among the patients.

We also evaluated the extent to which Tax-specific $CD4^+$ T cells were responsible for IFN-γ in the GST–Tax-based immunoassay system. We used PBMCs from patients #350 and #341, who showed high Tax-specific T cell responses. $CD8^+$ cell–depleted PBMCs from patient #350 and #341 showed a reduced but still significant level of Tax-specific IFN-γ–producing response compared with whole PBMCs (Fig. 1B). These results indicate that not only $CD8^+$ but also $CD4^+$ T cells against Tax are present in the peripheral blood from patient #350 and #341 after allo-HSCT with RIC.

Induction of an HTLV-1–specific $CD4^+$ T cell line from patient #350

We next attempted to induce HTLV-1–specific $CD4^+$ T cells from the PBMCs of patient #350 at 180 d after allo-HSCT, using an HTLV-1–infected T cell line (ILT-#350) as APCs. Freshly isolated PBMCs were stimulated for 2 wk with Tax301–309, a dominant CTL epitope presented by HLA-A*2402, to eliminate HTLV-1–infected cells, which potentially existed in PBMCs. The $CD4^+$ cells were then isolated from the cultured cells and stimulated with formaldehyde-fixed ILT-#350 every 2–3 wk. The established cell line was found to be a $CD4^+$ T cell line (designated as T4 cells thereafter) because cells expressed CD3 and CD4 but not CD8

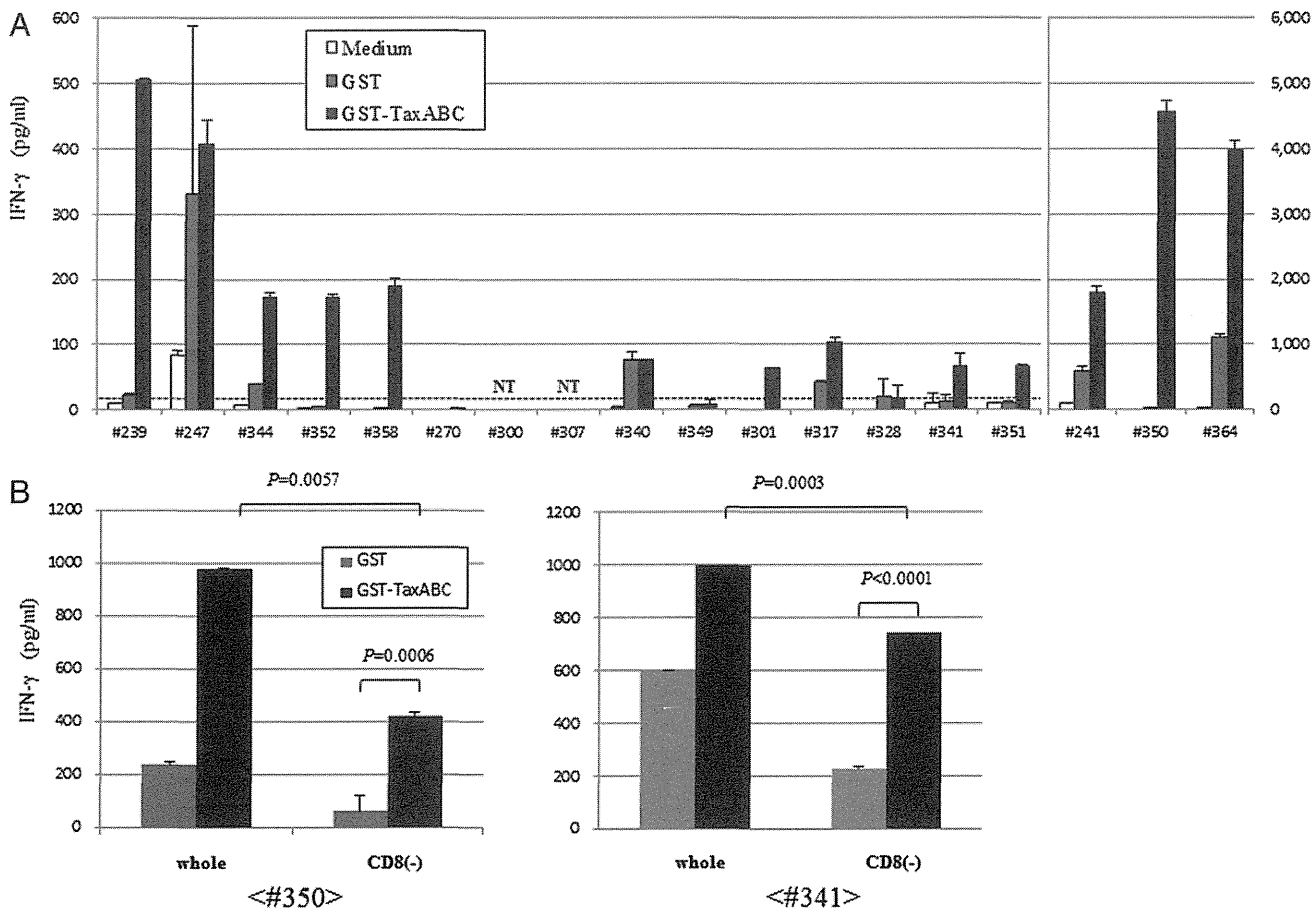

FIGURE 1. Diversity of Tax-specific T cell responses in ATL patients who received allo-HSCT with RIC. (**A** and **B**) PBMCs from 18 ATL patients at 180 d after allo-HSCT (A) or whole and $CD8^+$ cell–depleted PBMCs from two patients at 540 d after allo-HSCT (#350 and #341) (B) were cultured for 4 d in the absence (open square) or presence of GST (gray square), or GST–Tax (black square) proteins. The concentration of IFN-γ in the supernatant was determined by ELISA. The *y*-axis on the right side indicates the results from three patients (#241, #350, and #364). The dotted horizontal line indicates the detection limit (23.5 pg/ml). The error bars represent SD of duplicated wells. The representative result of two independent experiments is shown in (B).

(Fig. 2A). Because HTLV-1 has been shown to preferentially infect $CD4^+$ T cells in vivo and in vitro (24), we examined HTLV-1 expression in T4 cells by RT-PCR (Fig. 2B). As expected, the T4 cells did not express HTLV-1 Tax, indicating that the cells were not infected with HTLV-1. We assessed expression of various cytokines in T4 cells (Fig. 2C). The T4 cells were stimulated with formaldehyde-fixed ILT-#350 or LCL-#350. The cells produced large amounts of IFN-γ and TNF-α and small amounts of IL-2, IL-4, and IL-10 in response to ILT-#350 but not against LCL-#350. IL-6 and IL-17A were not detected in the culture supernatant. These data indicate that T4 cells are mainly HTLV-1–specific $CD4^+$ Th1-like cells but contain minor populations to produce Th2 cytokines.

Determination of the minimum epitope recognized by T4 cells

Freshly isolated PBMCs in the patient #350 produced IFN-γ in response to GST–Tax (Fig. 1A). We expected that the epitope recognized by the T4 cells should be present in the Tax protein. We therefore examined whether the T4 line responded to Tax using LCL-#350 pulsed with GST–Tax proteins as APCs. As shown in Fig. 3A, the T4 cells produced significantly higher amounts of IFN-γ in response to GST–TaxABC and GST–Tax-B (residues 113–237) (31) but not GST–Tax-A (residues 1–127) (31) and -C (residues 224–353 (31), when compared with the GST control protein, indicating that the T4 cells recognized the central region (residues 113–237) of the Tax Ag. We next synthesized eight overlapping 25-mer peptides spanning the central region of Tax (residues 103–246) and analyzed their abilities to stimulate T4 cells (Table II). The cell line produced high amounts of IFN-γ only when stimulated with Tax154–178 (Fig. 3B). We then prepared four overlapping 15-mer peptides, covering residues 154–178 of Tax, to examine the IFN-γ responses of the T4 cells (Table II). Both Tax151–165 and Tax156–170-stimulated cells to induce IFN-γ responses but not at a comparable level to Tax154–178 (Fig. 3C). These results suggest that the epitope recognized by T4 cells might be present in the N-terminal half of Tax154–178. We therefore stimulated the cells with Tax154–168, Tax155–169, or Tax156–170. The cells showed higher IFN-γ responses against Tax154–168 and Tax155–169 than Tax156–170, indicating that the minimum epitope might be within residues 155–168 of Tax (Fig. 3D). To identify the minimum epitope recognized by T4 cells, we next synthesized three overlapping peptides of 12- to 14-mer lengths beginning at residue 155 of Tax (Table II). Tax155–167 induced IFN-γ responses in cells at a similar level to Tax155–169 and Tax155–168, although Tax155–166 did not (Fig. 3E). Moreover, IFN-γ production of cells in response to various concentrations of Tax155–167 was comparable to that against Tax155–169 and Tax155–168 (Fig. 3F). These data clearly show that the minimum epitope recognized by the T4 cells is Tax155–167.

*HLA-DRB1*0101 restriction of Tax-specific T4 cells*

To analyze HLA class II molecules involved in the presentation of the minimum epitope, T4 cells were stimulated with ILT-#350 in the presence or absence of anti–HLA-DR, -DQ, and anti-HLA class I blocking Abs. As shown in Fig. 4A, the addition of an anti–HLA-DR blocking Ab abrogated IFN-γ responses of the T4 cells against ILT#-350, indicating that the epitope was HLA-DR restricted.

We further investigated the HLA-DR alleles responsible for the presentation of the minimum epitope by using four HLA-typed LCLs displaying different HLA-DRs. As shown in Fig. 4B, the T4 cells responded by producing IFN-γ when Tax155–167 was presented by autologous LCL-#350 (DR1/14) and allogeneic LCL-#341 (DR1/15). These results clearly indicate that this epitope is presented by HLA-DRB1*0101 on APCs. We searched for a known HLA-DRB1*0101 motif in the identified epitope Tax155–167 and found that this epitope contained the HLA-DRB1*0101 motif (Fig. 4C) (33).

Enhancement of Tax-specific $CD8^+$ T cell expansion by Tax155–167-specific $CD4^+$ T cell help

As T4 cells were established from PBMCs of an HTLV-1–infected patient #350, it is suggested that Tax155–167-specific $CD4^+$ T cells may be maintained in the HLA-DRB1*0101$^+$ patient #350.

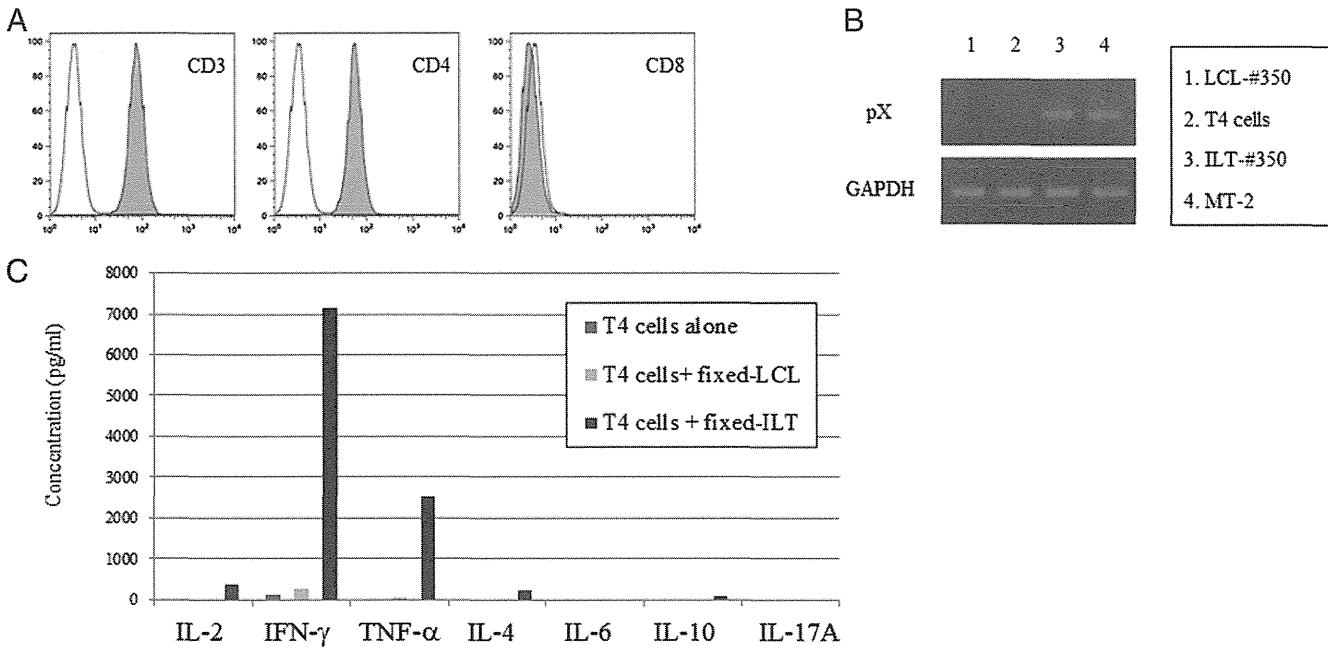

FIGURE 2. Phenotype and function of $CD4^+$ T cell line (T4) generated from patient #350. (**A**) Cell surface phenotype of T4 cells was analyzed by flow cytometry. (**B**) Total RNA was extracted from LCL-#350 (*lane 1*), T4 cells (*lane 2*), ILT-#350 (*lane 3*), and MT-2 (*lane 4*). Tax mRNA expression for each cell type was analyzed by RT-PCR. GAPDH was used as an internal control. (**C**) T4 cells were stimulated for 24 h with or without formaldehyde-fixed ILT-#350 or LCL-#350 cells. The concentration of indicated cytokines in the supernatants was measured using a cytometric bead array system.

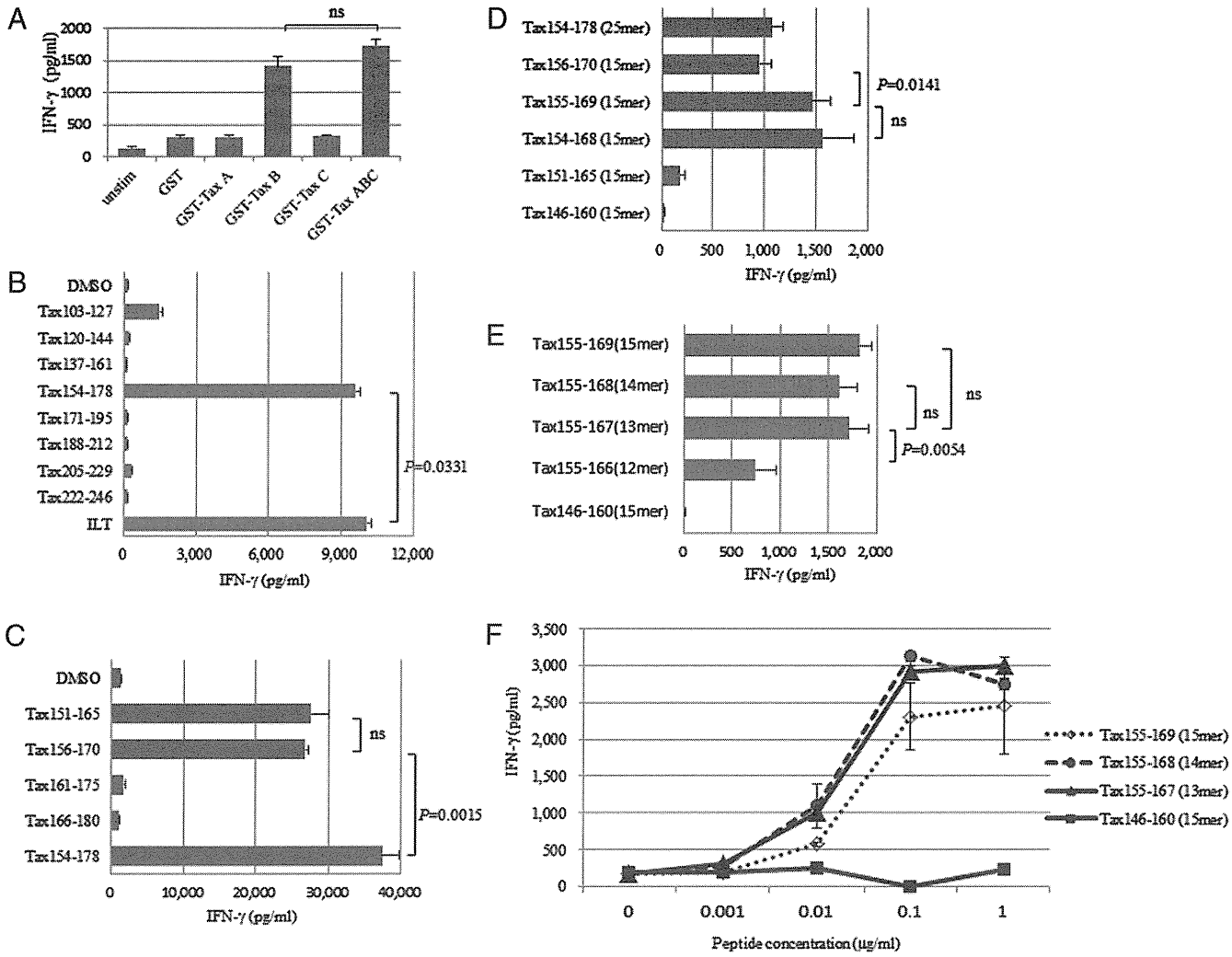

FIGURE 3. Identification of the dominant Tax-derived epitope recognized by established T4 cells. (**A**) Donor-derived LCL-#350 was pulsed with GST, GST–Tax-A, GST–Tax-B, GST–Tax-C, or a mixture of GST–Tax-A, -B, and -C (GST–TaxABC) for 24 h and then cocultured for 24 h with the T4 cells at a responder/stimulator (R/S) ratio of 3. IFN-γ production from T4 cells was analyzed by ELISA. (**B** and **C**) LCL-#350 was pulsed with the indicated overlapping 25-mer-long (B) or 15-mer-long (C) synthetic peptides (10 μg/ml) within the Tax-B region for 1 h. Formaldehyde-fixed ILT-#350 cells were cocultured with T4 cells for 6 h. IFN-γ in the supernatant was measured by ELISA. (**D** and **E**) IFN-γ responses of T4 cells were assessed using the indicated overlapping 12- to 25-mer-long synthetic peptides (100 ng/ml). (**F**) IFN-γ responses of T4 cells against indicated concentrations of 13- to 15-mer-long peptides were assessed as in (B) and (C). (A–F) Results are representative of two or three independent experiments. The error bars represent SD of triplicate wells. Statistical significance was analyzed by the unpaired *t* test.

We therefore evaluated the helper function of Tax155–167-specific $CD4^+$ T cells on the expansion of dominant Tax-specific CTLs in fresh PBMCs of the patient #350. Freshly isolated PBMCs from patient #350 (A24/26, DR1/14) at 540 d after allo-HSCT were stimulated for 13 d with the HLA-A24–restricted CTL epitope peptide (Tax301–309) in the presence or absence of the HLA-DRB1*0101–restricted $CD4^+$ Th epitope peptide (Tax155–167), and Tax-specific $CD8^+$ T cell expansion was evaluated using the HLA-A*2402/Tax301–309 tetramer. As shown in Fig. 5, Tax301–309-specific $CD8^+$ T cells proliferated to 9.26% of $CD8^+$ T cells when stimulated with Tax301–309 alone. Surprisingly, a highly elevated frequency (62.3%) of tetramer-binding $CD8^+$ T cells was detected by in vitro costimulation with Tax301–309 and Tax155–167, suggesting the presence of Tax155–167-specific $CD4^+$ Th cells in patient #350.

We examined whether Tax155–167-specific $CD4^+$ T cells existed and functioned as helper cells in the other two HTLV-1–infected HLA-DRB1*0101^+ patients after allo-HSCT (day 360 for patient #341 and day180 for #364). These patients had detectable levels of HLA-A*2402/Tax301–309 tetramer-binding $CD8^+$ T cells in the peripheral blood (Fig. 5). In patients #341 and #364, the tetramer-binding cells expanded to 7.7 and 0.849% of $CD8^+$ T cells at 13 d of culture when stimulated with the CTL epitope peptide, Tax301–309, alone. Costimulation of PBMCs with both peptides Tax155–167 and Tax301–309 led to a vigorous proliferation of tetramer-binding $CD8^+$ T cells (59.6% for patient #341 and 15.5% for patient #364) as observed in patient #350 (Fig. 5). These results indicate that Tax155–167-specific $CD4^+$ T cells may be present and contribute to enhancing $CD8^+$ T cell responses in HTLV-1–infected HLA-DRB1*0101^+ individuals after allo-HSCT.

*Tax155–167-specific $CD4^+$ T cells were maintained in HTLV-1–infected HLA-DRB1*0101^+ individuals*

We next generated the HLA-DRB1*0101/Tax155–167 tetramer to directly detect Tax155–167-specific $CD4^+$ T cells and examined the presence of Tax155–167-specific $CD4^+$ T cells in the PBMCs freshly isolated from two HLA-DRB1*0101^+ patients after allo-HSCT (day 180 for patient #350 and day 360 for patient #364).

Table II. Synthetic oligopeptides used in this study

Peptide	Sequence
Tax103–127	P S F L Q A M R K Y S P F R N G Y M E P T L G Q H
Tax120–144	M E P T L G Q H L P T L S F P D P G L R P Q N L Y
Tax137–161	G L R P Q N L Y T L W G G S V V C M Y L Y Q L S P
Tax154–178	M Y L Y Q L S P P I T W P L L P H V I F C H P G Q
Tax171–195	V I F C H P G Q L G A F L T N V P Y K R I E E L L
Tax188–212	Y K R I E E L L Y K I S L T T G A L I I L P E D C
Tax205–229	L I I L P E D C L P T T L F Q P A R A P V T L T A
Tax222–246	R A P V T L T A W Q N G L L P F H S T L T T P G I
Tax146–160	L W G G S V V C M Y L Y Q L S
Tax151–165	V V C M Y L Y Q L S P P I T W
Tax154–168	M Y L Y Q L S P P I T W P L L
Tax155–169	Y L Y Q L S P P I T W P L L P
Tax156–170	L Y Q L S P P I T W P L L P H
Tax161–175	P P I T W P L L P H V I F C H
Tax166–180	P L L P H V I F C H P G Q L G
Tax155–168	Y L Y Q L S P P I T W P L L
Tax155–167	Y L Y Q L S P P I T W P L
Tax155–166	Y L Y Q L S P P I T W P

Tax155–167-specific CD4$^+$ T cells were detected ex vivo in the patient #350 (0.11%) and proliferated to 11.6% among CD4$^+$ T cells at 13 d poststimulation with Tax155–167 peptide. In the patient #364, tetramer-binding CD4$^+$ T cells were undetectable in fresh PBMCs but expanded to 0.37% by in vitro stimulation with Tax155–167 peptide (Fig. 6A). In an HLA-DRB1*0101$^+$–seronegative donor #365, Tax155–167-specific CD4$^+$ T cells were not found in fresh PBMCs and did not become detectable at 13 d after stimulation with Tax155–167 peptide (Fig. 6A). This result indicates that Tax155–167-specific CD4$^+$ T cells are maintained and possesses the abilities to proliferate in response to HTLV-1 Tax in these patients.

We further examined whether Tax155–167-specific CD4$^+$ T cells existed in two HTLV-1–infected individuals carrying HLA-DRB1*0101, an AC #310 and a HAM/TSP patient #294, and detected 0.18 and 0.31% of tetramer-binding cells in peripheral CD4$^+$ T cells, respectively (Fig. 6B). These results suggest that Tax155–167-specific CD4$^+$ T cells are maintained in HTLV-1–infected individuals expressing an HLA-DRB1*0101 allele, regardless of HSCT.

Discussion

In this study, we demonstrated Tax-specific CD4$^+$ T cell responses in some ATL patients post–allo-HSCT and identified a novel HLA-DRB1*0101–restricted CD4 T cell epitope, Tax155–167, which was recognized by HTLV-1–specific CD4$^+$ T cells and consequently led to robust Tax-specific CD8$^+$ T cell expansion. We also found that Tax155–167-specific CD4$^+$ T cells existed in all HTLV-1–infected HLA-DRB1*0101$^+$ individuals tested, regardless of HSCT, by newly generated HLA-DRB1*0101/Tax155–167 tetramers. These results suggest that Tax155–167 might be a dominant epitope recognized by HTLV-1–specific CD4$^+$ T cells

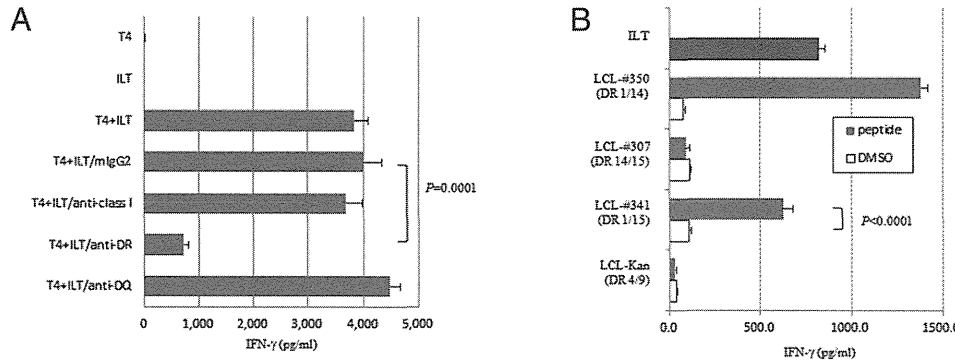

C

	Relative position												
	1	2	3	4	5	6	7	8	9	10	11	12	13
Tax155-167	Y	L	Y	Q	L	S	P	P	I	T	W	P	L
Anchor residues	Y,V, L,F, I,A M,W	*	*	L,A, I,V, M,N, Q	*	A,G, S,T, P	*	*	L,A, I,V, N,F, Y				

FIGURE 4. HLA-DRB1*0101 restriction of Tax155–167 recognition by established T4 cells. (**A**) T4 cells were cocultured for 6 h with ILT-#350 in the presence or absence of the following blocking Abs (10 μg/ml): anti-human HLA-DR; anti-human HLA-DQ; anti–HLA-class I; or isotype control. IFN-γ production from T4 cells was measured by ELISA. (**B**) The T4 cells were cocultured for 6 h with autologous (#350) or allogeneic (#307, #341, and Kan) LCLs pulsed with (closed bar) or without (open bar) Tax155–167 for 1 h or with recipient-derived ILT-#350. The HLA-DR alleles of each LCL line are indicated in parentheses. IFN-γ production of T4 cells was assessed by ELISA. (A and B) Representative data of three independent experiments are shown. The error bars represent SD of triplicate wells. Statistical significance was analyzed by the unpaired *t* test. (**C**) The amino acid sequence between residues 155 and 167 of Tax contained a putative HLA-DRB1*0101 anchor motif (33).

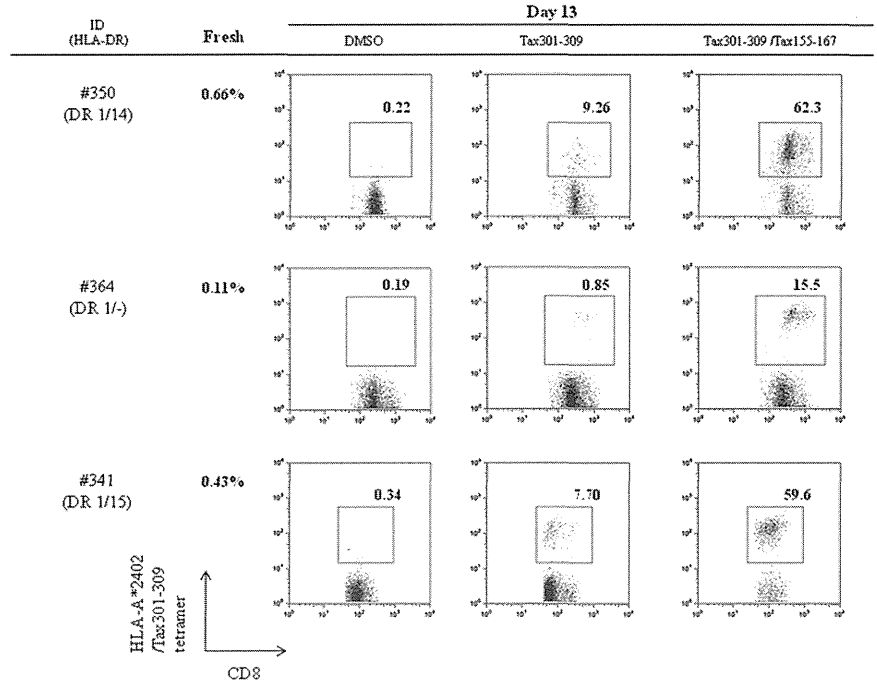

FIGURE 5. Augmentation of Tax-specific $CD8^+$ T cell expansion by costimulation with CTL epitope and Tax155–167 peptides. PBMCs from HLA-DRB1*0101– and HLA-A24–expressing ATL patients (#350, #364, and #341) who underwent allo-HSCT with RIC were cultured for 13 d in the presence of DMSO, 100 nM CTL epitope (Tax301–309), or a mixture of Tax301–309 (100 nM) and Tax155–167 (100 nM) peptides. Data indicate percentages of HLA-A*2402/Tax301–309 $tetramer^+$ cells among $CD3^+CD8^+$ T cells. Fresh indicates frequency of HLA-A*2402/Tax301–309 $tetramer^+CD8^+$ T cells detected in fresh peripheral blood.

in HTLV-1–infected individuals expressing HLA-DRB1*0101 and that Tax-specific $CD4^+$ T cells might efficiently induce HTLV-1–specific CTL expansion to strengthen the graft-versus-ATL effects in ATL patients after allo-HSCT.

In HTLV-1 infection, analysis of virus-specific $CD4^+$ T cell responses appears to be limited because $CD4^+$ T cells are preferentially infected with HTLV-1 (24, 34, 35), and HTLV-1 Ags are produced from infected cells at a few hours postculture (34, 36). In this study, we used blood samples from 18 ATL patients after allo-HSCT with RIC and from HLA identical–related or unrelated donors and found that these recipients had undetectable or very low proviral loads (Table I), as previously shown (7–9). We previously reported that Tax-specific CTLs were induced in some patients with complete remission after allo-HSCT for ATL and might contribute to the graft-versus-leukemia effect (10). In the current study, Tax-specific T cell responses or tetramer-binding $CD8^+$ T cells were detected in 68.8% (11 of 16) or 82.4% (14 of 17) of patients tested, respectively (Fig. 1A, Table I). In addition, helper function of Tax-specific $CD4^+$ T cells to enhance Tax-specific $CD8^+$ T cell expansion was observed in PBMCs from all three HLA-DRB1*0101$^+$ patients tested (Fig. 5). These data suggest that both $CD8^+$ and $CD4^+$ Tax-specific T cell responses might contribute to elimination of remaining leukemic and/or infected cells in some patients having T cell responses against Tax. However, given the fact that not all ATL patients who achieved complete remission after allo-HSCT had Tax-specific $CD8^+$ T cells, graft-versus-host reaction may mainly contribute to achieve complete remission after allo-HSCT. It is of note that Tax-specific

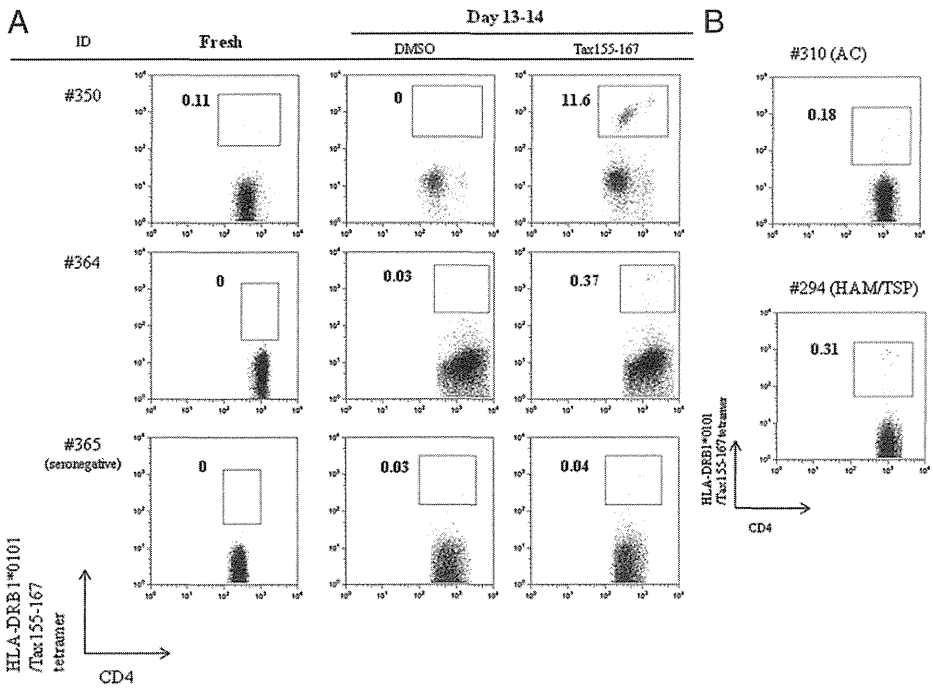

FIGURE 6. Detection of Tax155–167-specific $CD4^+$ T cells in HTLV-1–infected HLA-DRB1*0101$^+$ individuals. (**A**) In two ATL patients after allo-HSCT (#350 and #364) and an HLA-DRB1*0101$^+$–seronegative donor (#365), frequency of HLA-DRB1*0101/Tax155–167 tetramer-binding $CD4^+$ T cells was analyzed in fresh PBMCs and PBMCs cultured for 13–14 d in the presence of Tax155–167 (100 nM) peptide. Data indicate percentages of $tetramer^+$ cells in $CD3^+CD4^+$ T cells. (**B**) Frequency of HLA-DRB1*0101/Tax155–167 tetramer-binding $CD4^+$ T cells in fresh PBMCs from an AC #310 and an HAM/TSP patient #294 was analyzed. Data indicate percentages of $tetramer^+$ cells in $CD3^+CD4^+$ T cells.

T cell responses were detected in 57.1% (four of seven) or 87.5% (seven of eight) of the patients after allo-HSCT with RIC from HTLV-1–seronegative sibling or unrelated donors, respectively. A Tax-specific T cell response was not detected in three patients who underwent allo-HSCT from seropositive donors (Fig. 1, Table I).

It has been proposed that CTLs are the main effector cells against many pathogenic viruses, including HTLV-1. To date, many CTL epitopes recognized by HTLV-1–specific CTLs have been identified, some of which are thought to be the candidates of peptide-based T cell immunotherapy (10, 20, 32, 37–40). $CD4^+$ T cells have also been known to be critical for induction and maintenance of Ag-specific $CD8^+$ T cells (15–19). With respect to HTLV-1 infection, there are several reports identifying HLA-DRB1*0101–restricted epitopes recognized by $CD4^+$ T cells against Env or Tax (Env380–394 (21), Env436–450, Env451–465, Env456–470 (23), and Tax191–205 (22)), which were established by stimulating PBMCs from uninfected or infected individuals with synthetic peptides. In this study, for determination of an epitope recognized by HTLV-1–specific $CD4^+$ T cells, we established an HTLV-1–specific $CD4^+$ T cell line from the patient #350 at 180 d after allo-HSCT by several stimulations with an HTLV-1 Ags-expressing T cell line (ILT-#350) from the same patient. In addition, we found that Tax155–167-specific $CD4^+$ T cells were present in peripheral blood from patient #350 at 180 and 540 d after all-HSCT, indicating that the epitope, Tax155–167, identified in this study is naturally presented on HTLV-1–infected cells and predominantly recognized by HTLV-1–specific $CD4^+$ Th cells in the patient #350 at least within 540 d after allo-HSCT. Another HLA-DRB1*0101–restricted Tax epitope, Tax191–205, has been reported previously (22). In this study, the amino acid sequence within this region was revealed to be conserved in the infected T cell line, ILT-#350 established from the patient #350 (data not shown), indicating that Tax191–205 can be presented on APCs and Tax191–205-specific $CD4^+$ T cells may be induced in patient #350. However, Tax155–167-specific but not Tax191–205-specific $CD4^+$ T cells were revealed to predominantly appear in the HTLV-1–specific T4 cell line, established from PBMCs in the patient #350 at 180 d after allo-HSCT. This suggests that in the case of patient #350 at 180 d after allo-HSCT, Tax191–205-specific $CD4^+$ T cells may not be the most frequent population among HTLV-1–specific $CD4^+$ T cells.

It has been known that Ag-specific effector and memory $CD4^+$ T cells are typically present at much lower frequencies than their $CD8^+$ counterparts and that MHC class II tetramer might have a weak TCR–MHC affinity (41). Although this limited affinity of MHC class II tetramer might preclude detection of Ag-specific low-affinity $CD4^+$ T cells, the low-affinity $CD4^+$ T cells, below detection with MHC class II tetramers, were also proved to be critical effectors in Ag-specific responses (42). In the current study, MHC class II tetramer analysis revealed that Tax155–167-specific $CD4^+$ T cells were present in HLA-DRB1*0101$^+$ HTLV-1–infected individuals: two ATL patients after allo-HSCT (day 180 for #350 and day 360 for #364), an AC #310, and a HAM/TSP patient #294 (Fig. 6). Because of a shortage of blood sample from patient #341, we could not perform the direct detection for Tax155–167-specific $CD4^+$ T cells by the MHC class II tetramers. However, enhanced expansion of Tax301–309-specific $CD8^+$ T cells was observed in patient #341 at 360 d after allo-HSCT when PBMCs were stimulated with Tax301–309 in the presence of Tax155–167 (Fig. 5). So far, Tax155–167-specific $CD4^+$ T cells were detected in fresh and/or Tax155–167-stimulated PBMCs of all HTLV-1–infected HLA-DRB1*0101$^+$ individuals tested, although their frequencies were various. These results suggest that Tax155–167 may be the dominant epitope recognized by Tax-specific $CD4^+$ T cells in HTLV-1–infected HLA-DRB1*0101$^+$ individuals. In ATL patients after HSCT, the donor-derived T cells reconstituted in recipients will first encounter HTLV-1 Ags, because HTLV-1 still persists in the patients even though proviral loads become undetectable in the peripheral bloods. Indeed, we found that donor-derived Tax155–167-specific $CD4^+$ T cells were present in three ATL patients after allo-HSCT from seronegative donors. This finding also suggests that Tax155–167-specific naive $CD4^+$ T cells may pre-exist in HLA-DRB1*0101$^+$ individuals and can be primed with HTLV-1 Ags during the primary infection. In this study, Tax155–167-specific $CD4^+$ T cells were also detected in an AC and a HAM/TSP patient (Fig. 6B), suggesting that Tax155–167-specific $CD4^+$ T cells may be maintained in some HLA-DR1$^+$ individuals during the chronic phase of HTLV-1 infection. However, it has been reported that epitope hierarchies may change because of T cell escape mutants (43, 44) and unresponsiveness or deletion of epitope-specific T cells because of prolonged Ag stimulation during chronic infection (45, 46). Further longitudinal studies with a number of samples will be required to confirm that Tax155–167 is a dominant epitope of HTLV-1–specific $CD4^+$ T cells in HLA-DRB1*0101$^+$–infected individuals in the course of HTLV-1 infection.

Among three patients (#241, #350, and #364) showing high T cell responses against recombinant Tax protein, two patients (#350 and #364) were found to carry HLA-DRB1*0101 and have efficient $CD4^+$ Th cell responses against Tax155–167. Intriguingly, it has been reported that HLA-DRB1*0101 is associated with susceptibility to HAM/TSP (47, 48). In addition, $CD4^+$ T cells have been shown to be the dominant cells infiltrating in early active inflammatory spinal cord lesions (28, 29) with spontaneous production of proinflammatory cytokines (30). These observations suggest that HLA-DRB1*0101 might be associated with susceptibility to HAM/TSP via an effect on high $CD4^+$ T cell activation. Further studies are needed to clarify whether HLA-DRB1*0101 is associated with high Tax-specific $CD4^+$ T cell responses in HTLV-1–infected individuals.

Early studies using lymphocytic choriomeningitis virus showed that $CD4^+$ T cell help is critical for maintenance of $CD8^+$ T cell function during chronic infections (18). It has also been suggested that $CD4^+$ T cells are required for optimal CTL responses during HTLV-1 infection (49). Aubert et al. (50) showed that both Ag-specific naive and effector $CD4^+$ T cell help rescued exhausted $CD8^+$ T cells in vivo, resulting in a decrease in viral burden. In the current study, we determined a novel HLA-DRB1*0101–restricted Th epitope, Tax155–167, which was capable of augmenting Tax-specific $CD8^+$ T cell expansion by stimulating Tax155–167-specific $CD4^+$ T cells. This epitope would be a useful tool for investigating the roles of HTLV-1–specific $CD4^+$ T cells in antitumor immunity and in pathogenesis of HTLV-1–related inflammatory diseases such as HAM/TSP and developing novel vaccines to prevent progression or recurrence of ATL.

Disclosures

The authors have no financial conflicts of interest.

References

1. Hinuma, Y., K. Nagata, M. Hanaoka, M. Nakai, T. Matsumoto, K. I. Kinoshita, S. Shirakawa, and I. Miyoshi. 1981. Adult T-cell leukemia: antigen in an ATL cell line and detection of antibodies to the antigen in human sera. *Proc. Natl. Acad. Sci. USA* 78: 6476–6480.
2. Poiesz, B. J., F. W. Ruscetti, A. F. Gazdar, P. A. Bunn, J. D. Minna, and R. C. Gallo. 1980. Detection and isolation of type C retrovirus particles from fresh and cultured lymphocytes of a patient with cutaneous T-cell lymphoma. *Proc. Natl. Acad. Sci. USA* 77: 7415–7419.

3. de Thé, G., and R. Bomford. 1993. An HTLV-I vaccine: why, how, for whom? *AIDS Res. Hum. Retroviruses* 9: 381–386.
4. Uchiyama, T. 1997. Human T cell leukemia virus type I (HTLV-I) and human diseases. *Annu. Rev. Immunol.* 15: 15–37.
5. Tsukasaki, K., T. Maeda, K. Arimura, J. Taguchi, T. Fukushima, Y. Miyazaki, Y. Moriuchi, K. Kuriyama, Y. Yamada, and M. Tomonaga. 1999. Poor outcome of autologous stem cell transplantation for adult T cell leukemia/lymphoma: a case report and review of the literature. *Bone Marrow Transplant.* 23: 87–89.
6. Utsunomiya, A., Y. Miyazaki, Y. Takatsuka, S. Hanada, K. Uozumi, S. Yashiki, M. Tara, F. Kawano, Y. Saburi, H. Kikuchi, et al. 2001. Improved outcome of adult T cell leukemia/lymphoma with allogeneic hematopoietic stem cell transplantation. *Bone Marrow Transplant.* 27: 15–20.
7. Tanosaki, R., N. Uike, A. Utsunomiya, Y. Saburi, M. Masuda, M. Tomonaga, T. Eto, M. Hidaka, M. Harada, I. Choi, et al. 2008. Allogeneic hematopoietic stem cell transplantation using reduced-intensity conditioning for adult T cell leukemia/lymphoma: impact of antithymocyte globulin on clinical outcome. *Biol. Blood Marrow Transplant.* 14: 702–708.
8. Choi, I., R. Tanosaki, N. Uike, A. Utsunomiya, M. Tomonaga, M. Harada, T. Yamanaka, M. Kannagi, and J. Okamura. 2011. Long-term outcomes after hematopoietic SCT for adult T-cell leukemia/lymphoma: results of prospective trials. *Bone Marrow Transplant.* 46: 116–118.
9. Okamura, J., A. Utsunomiya, R. Tanosaki, N. Uike, S. Sonoda, M. Kannagi, M. Tomonaga, M. Harada, N. Kimura, M. Masuda, et al. 2005. Allogeneic stem-cell transplantation with reduced conditioning intensity as a novel immunotherapy and antiviral therapy for adult T-cell leukemia/lymphoma. *Blood* 105: 4143–4145.
10. Harashima, N., K. Kurihara, A. Utsunomiya, R. Tanosaki, S. Hanabuchi, M. Masuda, T. Ohashi, F. Fukui, A. Hasegawa, T. Masuda, et al. 2004. Graft-versus-Tax response in adult T-cell leukemia patients after hematopoietic stem cell transplantation. *Cancer Res.* 64: 391–399.
11. Jacobson, S., H. Shida, D. E. McFarlin, A. S. Fauci, and S. Koenig. 1990. Circulating $CD8^+$ cytotoxic T lymphocytes specific for HTLV-I pX in patients with HTLV-I associated neurological disease. *Nature* 348: 245–248.
12. Kannagi, M., S. Harada, I. Maruyama, H. Inoko, H. Igarashi, G. Kuwashima, S. Sato, M. Morita, M. Kidokoro, M. Sugimoto, et al. 1991. Predominant recognition of human T cell leukemia virus type I (HTLV-I) pX gene products by human $CD8^+$ cytotoxic T cells directed against HTLV-I-infected cells. *Int. Immunol.* 3: 761–767.
13. Shimizu, Y., A. Takamori, A. Utsunomiya, M. Kurimura, Y. Yamano, M. Hishizawa, A. Hasegawa, F. Kondo, K. Kurihara, N. Harashima, et al. 2009. Impaired Tax-specific T-cell responses with insufficient control of HTLV-1 in a subgroup of individuals at asymptomatic and smoldering stages. *Cancer Sci.* 100: 481–489.
14. Takamori, A., A. Hasegawa, A. Utsunomiya, Y. Maeda, Y. Yamano, M. Masuda, Y. Shimizu, Y. Tamai, A. Sasada, N. Zeng, et al. 2011. Functional impairment of Tax-specific but not cytomegalovirus-specific $CD8^+$ T lymphocytes in a minor population of asymptomatic human T-cell leukemia virus type 1-carriers. *Retrovirology* 8: 100.
15. Cardin, R. D., J. W. Brooks, S. R. Sarawar, and P. C. Doherty. 1996. Progressive loss of $CD8^+$ T cell-mediated control of a gamma-herpesvirus in the absence of $CD4^+$ T cells. *J. Exp. Med.* 184: 863–871.
16. Grakoui, A., N. H. Shoukry, D. J. Woollard, J. H. Han, H. L. Hanson, J. Ghrayeb, K. K. Murthy, C. M. Rice, and C. M. Walker. 2003. HCV persistence and immune evasion in the absence of memory T cell help. *Science* 302: 659–662.
17. Kalams, S. A., S. P. Buchbinder, E. S. Rosenberg, J. M. Billingsley, D. S. Colbert, N. G. Jones, A. K. Shea, A. K. Trocha, and B. D. Walker. 1999. Association between virus-specific cytotoxic T-lymphocyte and helper responses in human immunodeficiency virus type 1 infection. *J. Virol.* 73: 6715–6720.
18. Matloubian, M., R. J. Concepcion, and R. Ahmed. 1994. $CD4^+$ T cells are required to sustain $CD8^+$ cytotoxic T-cell responses during chronic viral infection. *J. Virol.* 68: 8056–8063.
19. Smyk-Pearson, S., I. A. Tester, J. Klarquist, B. E. Palmer, J. M. Pawlotsky, L. Golden-Mason, and H. R. Rosen. 2008. Spontaneous recovery in acute human hepatitis C virus infection: functional T-cell thresholds and relative importance of CD4 help. *J. Virol.* 82: 1827–1837.
20. Jacobson, S., J. S. Reuben, R. D. Streilein, and T. J. Palker. 1991. Induction of $CD4^+$, human T lymphotropic virus type-1-specific cytotoxic T lymphocytes from patients with HAM/TSP: recognition of an immunogenic region of the gp46 envelope glycoprotein of human T lymphotropic virus type-1. *J. Immunol.* 146: 1155–1162.
21. Kitze, B., K. Usuku, Y. Yamano, S. Yashiki, M. Nakamura, T. Fujiyoshi, S. Izumo, M. Osame, and S. Sonoda. 1998. Human $CD4^+$ T lymphocytes recognize a highly conserved epitope of human T lymphotropic virus type 1 (HTLV-1) env gp21 restricted by HLA DRB1*0101. *Clin. Exp. Immunol.* 111: 278–285.
22. Kobayashi, H., T. Ngato, K. Sato, N. Aoki, S. Kimura, Y. Tanaka, H. Aizawa, M. Tateno, and E. Celis. 2006. In vitro peptide immunization of target tax protein human T-cell leukemia virus type 1-specific $CD4^+$ helper T lymphocytes. *Clin. Cancer Res.* 12: 3814–3822.
23. Yamano, Y., B. Kitze, S. Yashiki, K. Usuku, T. Fujiyoshi, T. Kaminagayoshi, K. Unoki, S. Izumo, M. Osame, and S. Sonoda. 1997. Preferential recognition of synthetic peptides from HTLV-I gp21 envelope protein by HLA-DRB1 alleles associated with HAM/TSP (HTLV-I-associated myelopathy/tropical spastic paraparesis). *J. Neuroimmunol.* 76: 50–60.
24. Goon, P. K., T. Igakura, E. Hanon, A. J. Mosley, A. Barfield, A. L. Barnard, L. Kaftantzi, Y. Tanaka, G. P. Taylor, J. N. Weber, and C. R. Bangham. 2004. Human T cell lymphotropic virus type I (HTLV-I)-specific $CD4^+$ T cells: immunodominance hierarchy and preferential infection with HTLV-I. *J. Immunol.* 172: 1735–1743.
25. Toulza, F., A. Heaps, Y. Tanaka, G. P. Taylor, and C. R. Bangham. 2008. High frequency of $CD4^+FoxP3^+$ cells in HTLV-1 infection: inverse correlation with HTLV-1-specific CTL response. *Blood* 111: 5047–5053.
26. Satou, Y., J. Yasunaga, M. Yoshida, and M. Matsuoka. 2006. HTLV-I basic leucine zipper factor gene mRNA supports proliferation of adult T cell leukemia cells. *Proc. Natl. Acad. Sci. USA* 103: 720–725.
27. Sugata, K., Y. Satou, J. Yasunaga, H. Hara, K. Ohshima, A. Utsunomiya, M. Mitsuyama, and M. Matsuoka. 2012. HTLV-1 bZIP factor impairs cell-mediated immunity by suppressing production of Th1 cytokines. *Blood* 119: 434–444.
28. Iwasaki, Y., Y. Ohara, I. Kobayashi, and S. Akizuki. 1992. Infiltration of helper/inducer T lymphocytes heralds central nervous system damage in human T-cell leukemia virus infection. *Am. J. Pathol.* 140: 1003–1008.
29. Umehara, F., S. Izumo, M. Nakagawa, A. T. Ronquillo, K. Takahashi, K. Matsumuro, E. Sato, and M. Osame. 1993. Immunocytochemical analysis of the cellular infiltrate in the spinal cord lesions in HTLV-I-associated myelopathy. *J. Neuropathol. Exp. Neurol.* 52: 424–430.
30. Umehara, F., S. Izumo, A. T. Ronquillo, K. Matsumuro, E. Sato, and M. Osame. 1994. Cytokine expression in the spinal cord lesions in HTLV-I-associated myelopathy. *J. Neuropathol. Exp. Neurol.* 53: 72–77.
31. Kurihara, K., Y. Shimizu, A. Takamori, N. Harashima, M. Noji, T. Masuda, A. Utsunomiya, J. Okamura, and M. Kannagi. 2006. Human T-cell leukemia virus type-I (HTLV-I)-specific T-cell responses detected using three-divided glutathione-*S*-transferase (GST)-Tax fusion proteins. *J. Immunol. Methods* 313: 61–73.
32. Harashima, N., R. Tanosaki, Y. Shimizu, K. Kurihara, T. Masuda, J. Okamura, and M. Kannagi. 2005. Identification of two new HLA-A*1101-restricted tax epitopes recognized by cytotoxic T lymphocytes in an adult T-cell leukemia patient after hematopoietic stem cell transplantation. *J. Virol.* 79: 10088–10092.
33. Rammensee, H. G., T. Friede, and S. Stevanoviíc. 1995. MHC ligands and peptide motifs: first listing. *Immunogenetics* 41: 178–228.
34. Hanon, E., S. Hall, G. P. Taylor, M. Saito, R. Davis, Y. Tanaka, K. Usuku, M. Osame, J. N. Weber, and C. R. Bangham. 2000. Abundant tax protein expression in $CD4^+$ T cells infected with human T-cell lymphotropic virus type I (HTLV-I) is prevented by cytotoxic T lymphocytes. *Blood* 95: 1386–1392.
35. Richardson, J. H., A. J. Edwards, J. K. Cruickshank, P. Rudge, and A. G. Dalgleish. 1990. In vivo cellular tropism of human T-cell leukemia virus type 1. *J. Virol.* 64: 5682–5687.
36. Sakai, J. A., M. Nagai, M. B. Brennan, C. A. Mora, and S. Jacobson. 2001. In vitro spontaneous lymphoproliferation in patients with human T-cell lymphotropic virus type I-associated neurologic disease: predominant expansion of $CD8^+$ T cells. *Blood* 98: 1506–1511.
37. Elovaara, I., S. Koenig, A. Y. Brewah, R. M. Woods, T. Lehky, and S. Jacobson. 1993. High human T cell lymphotropic virus type 1 (HTLV-1)-specific precursor cytotoxic T lymphocyte frequencies in patients with HTLV-1-associated neurological disease. *J. Exp. Med.* 177: 1567–1573.
38. Kannagi, M., H. Shida, H. Igarashi, K. Kuruma, H. Murai, Y. Aono, I. Maruyama, M. Osame, T. Hattori, H. Inoko, et al. 1992. Target epitope in the Tax protein of human T-cell leukemia virus type I recognized by class I major histocompatibility complex-restricted cytotoxic T cells. *J. Virol.* 66: 2928–2933.
39. Pique, C., A. Ureta-Vidal, A. Gessain, B. Chancerel, O. Gout, R. Tamouza, F. Agis, and M. C. Dokhélar. 2000. Evidence for the chronic in vivo production of human T cell leukemia virus type I Rof and Tof proteins from cytotoxic T lymphocytes directed against viral peptides. *J. Exp. Med.* 191: 567–572.
40. Sundaram, R., Y. Sun, C. M. Walker, F. A. Lemonnier, S. Jacobson, and P. T. Kaumaya. 2003. A novel multivalent human CTL peptide construct elicits robust cellular immune responses in HLA-A*0201 transgenic mice: implications for HTLV-1 vaccine design. *Vaccine* 21: 2767–2781.
41. Vollers, S. S., and L. J. Stern. 2008. Class II major histocompatibility complex tetramer staining: progress, problems, and prospects. *Immunology* 123: 305–313.
42. Sabatino, J. J., Jr., J. Huang, C. Zhu, and B. D. Evavold. 2011. High prevalence of low affinity peptide-MHC II tetramer-negative effectors during polyclonal $CD4^+$ T cell responses. *J. Exp. Med.* 208: 81–90.
43. Goulder, P. J., A. K. Sewell, D. G. Lalloo, D. A. Price, J. A. Whelan, J. Evans, G. P. Taylor, G. Luzzi, P. Giangrande, R. E. Phillips, and A. J. McMichael. 1997. Patterns of immunodominance in HIV-1-specific cytotoxic T lymphocyte responses in two human histocompatibility leukocyte antigens (HLA)-identical siblings with HLA-A*0201 are influenced by epitope mutation. *J. Exp. Med.* 185: 1423–1433.
44. Nowak, M. A., R. M. May, R. E. Phillips, S. Rowland-Jones, D. G. Lalloo, S. McAdam, P. Klenerman, B. Köppe, K. Sigmund, C. R. Bangham, et al. 1995. Antigenic oscillations and shifting immunodominance in HIV-1 infections. *Nature* 375: 606–611.
45. Goulder, P. J., M. A. Altfeld, E. S. Rosenberg, T. Nguyen, Y. Tang, R. L. Eldridge, M. M. Addo, S. He, J. S. Mukherjee, M. N. Phillips, et al. 2001. Substantial differences in specificity of HIV-specific cytotoxic T cells in acute and chronic HIV infection. *J. Exp. Med.* 193: 181–194.
46. Wherry, E. J., J. N. Blattman, K. Murali-Krishna, R. van der Most, and R. Ahmed. 2003. Viral persistence alters CD8 T-cell immunodominance and tissue distribution and results in distinct stages of functional impairment. *J. Virol.* 77: 4911–4927.
47. Jeffery, K. J., K. Usuku, S. E. Hall, W. Matsumoto, G. P. Taylor, J. Procter, M. Bunce, G. S. Ogg, K. I. Welsh, J. N. Weber, et al. 1999. HLA alleles de-

termine human T-lymphotropic virus-I (HTLV-I) proviral load and the risk of HTLV-I-associated myelopathy. *Proc. Natl. Acad. Sci. USA* 96: 3848–3853.
48. Sabouri, A. H., M. Saito, K. Usuku, S. N. Bajestan, M. Mahmoudi, M. Forughipour, Z. Sabouri, Z. Abbaspour, M. E. Goharjoo, E. Khayami, et al. 2005. Differences in viral and host genetic risk factors for development of human T-cell lymphotropic virus type 1 (HTLV-1)-associated myelopathy/tropical spastic paraparesis between Iranian and Japanese HTLV-1-infected individuals. *J. Gen. Virol.* 86: 773–781.
49. Kurihara, K., N. Harashima, S. Hanabuchi, M. Masuda, A. Utsunomiya, R. Tanosaki, M. Tomonaga, T. Ohashi, A. Hasegawa, T. Masuda, et al. 2005. Potential immunogenicity of adult T cell leukemia cells in vivo. *Int. J. Cancer* 114: 257–267.
50. Aubert, R. D., A. O. Kamphorst, S. Sarkar, V. Vezys, S. J. Ha, D. L. Barber, L. Ye, A. H. Sharpe, G. J. Freeman, and R. Ahmed. 2011. Antigen-specific CD4 T-cell help rescues exhausted CD8 T cells during chronic viral infection. *Proc. Natl. Acad. Sci. USA* 108: 21182–21187.

HIV-1 Vpr Accelerates Viral Replication during Acute Infection by Exploitation of Proliferating CD4$^+$ T Cells *In Vivo*

Kei Sato[1,2]*, Naoko Misawa[1], Shingo Iwami[3,4], Yorifumi Satou[5], Masao Matsuoka[5], Yukihito Ishizaka[6], Mamoru Ito[7], Kazuyuki Aihara[8,9], Dong Sung An[10,11,12], Yoshio Koyanagi[1,2]*

1 Laboratory of Virus Pathogenesis, Institute for Virus Research, Kyoto University, Kyoto, Kyoto, Japan, **2** Center for Emerging Virus Research, Institute for Virus Research, Kyoto University, Kyoto, Kyoto, Japan, **3** Department of Biology, Faculty of Sciences, Kyushu University, Fukuoka, Fukuoka, Japan, **4** Precursory Research for Embryonic Science and Technology (PRESTO), Japan Science and Technology Agency (JST), Kawaguchi, Saitama, Japan, **5** Laboratory of Viral Control, Institute for Virus Research, Kyoto University, Kyoto, Kyoto, Japan, **6** Department of Intractable Diseases, National Center for Global Health and Medicine, Shinjuku-ku, Tokyo, Japan, **7** Central Institute for Experimental Animals, Kawasaki, Kanagawa, Japan, **8** Institute of Industrial Science, The University of Tokyo, Meguro-ku, Tokyo, Japan, **9** Graduate School of Information Science and Technology, The University of Tokyo, Meguro-ku, Tokyo, Japan, **10** Division of Hematology-Oncology, University of California, Los Angeles (UCLA), Los Angeles, California, United States of America, **11** School of Nursing, UCLA, Los Angeles, California, United States of America, **12** AIDS Institute, UCLA, Los Angeles, California, United States of America

Abstract

The precise role of viral protein R (Vpr), an HIV-1-encoded protein, during HIV-1 infection and its contribution to the development of AIDS remain unclear. Previous reports have shown that Vpr has the ability to cause G_2 cell cycle arrest and apoptosis in HIV-1-infected cells *in vitro*. In addition, *vpr* is highly conserved in transmitted/founder HIV-1s and in all primate lentiviruses, which are evolutionarily related to HIV-1. Although these findings suggest an important role of Vpr in HIV-1 pathogenesis, its direct evidence *in vivo* has not been shown. Here, by using a human hematopoietic stem cell-transplanted humanized mouse model, we demonstrated that Vpr causes G_2 cell cycle arrest and apoptosis predominantly in proliferating CCR5$^+$ CD4$^+$ T cells, which mainly consist of regulatory CD4$^+$ T cells (Tregs), resulting in Treg depletion and enhanced virus production during acute infection. The Vpr-dependent enhancement of virus replication and Treg depletion is observed in CCR5-tropic but not CXCR4-tropic HIV-1-infected mice, suggesting that these effects are dependent on the coreceptor usage by HIV-1. Immune activation was observed in CCR5-tropic wild-type but not in *vpr*-deficient HIV-1-infected humanized mice. When humanized mice were treated with denileukin diftitox (DD), to deplete Tregs, DD-treated humanized mice showed massive activation/proliferation of memory T cells compared to the untreated group. This activation/proliferation enhanced CCR5 expression in memory CD4$^+$ T cells and rendered them more susceptible to CCR5-tropic wild-type HIV-1 infection than to *vpr*-deficient virus. Taken together, these results suggest that Vpr takes advantage of proliferating CCR5$^+$ CD4$^+$ T cells for enhancing viremia of CCR5-tropic HIV-1. Because Tregs exist in a higher cycling state than other T cell subsets, Tregs appear to be more vulnerable to exploitation by Vpr during acute HIV-1 infection.

Citation: Sato K, Misawa N, Iwami S, Satou Y, Matsuoka M, et al. (2013) HIV-1 Vpr Accelerates Viral Replication during Acute Infection by Exploitation of Proliferating CD4$^+$ T Cells *In Vivo*. PLoS Pathog 9(12): e1003812. doi:10.1371/journal.ppat.1003812

Editor: Jeremy Luban, University of Massachusetts Medical School, United States of America

Received June 17, 2013; **Accepted** October 22, 2013; **Published** December 5, 2013

Funding: This work was supported in part by grants from the following: Grants-in-Aid for Scientific Research B21390137 (to YK) and S22220007 (to MI and YK) and a Grant-in-Aid for Young Scientists B23790500 (to KS) from the Japan Society for the Promotion of Science (JSPS); grants from Research on Emerging and Reemerging Infectious Diseases (to YK) and Research on HIV/AIDS (to YK) from the Ministry of Health, Labor and Welfare of Japan; a grant from the Uehara Memorial Foundation (to KS); the Shimizu Foundation for Immunological Research Grant (to KS); Takeda Science Foundation (to KS); JST PRESTO program (to SI); and a UCLA CFAR grant 5P30AI028697 (to DSA). This research was also supported by the Aihara Innovative Mathematical Modelling Project, JSPS through the "Funding Program for World-Leading Innovative R&D on Science and Technology (FIRST Program)," initiated by the Council for Science and Technology Policy (to KS, SI, and KA). The funders had no role in study design, data collection and analysis, decision to publish, or preparation of the manuscript.

Competing Interests: The authors have declared that no competing interests exist.

* E-mail: ksato@virus.kyoto-u.ac.jp (KS); ykoyanag@virus.kyoto-u.ac.jp (YK)

Introduction

Human immunodeficiency virus type 1 (HIV-1), the causative agent of acquired immunodeficiency syndrome (AIDS), encodes four viral accessory proteins: Vif, Vpu, Nef, and Vpr. Vpr is a small (96 amino acids) but multipotent protein which is known to induce G_2 cell cycle arrest, apoptosis, and the enhancement of HIV-1 long terminal repeat (LTR)-driven transcription in infected cells [1]. Previous *in vitro* studies have reported that *vpr*-deficient HIV-1 is less replicative in CD4$^+$ T cell lines [2] and cycling primary CD4$^+$ T cells [3]. On the other hand, *vpr* deficiency modestly affects viral replication kinetics in tonsil histocultures in which resting CD4$^+$ T cells dominantly reside [4]. *In vivo*, *vpr*-deficient SIV is less replicative but induces AIDS in macaque monkeys [5]. However, although the underlying molecular mechanisms of Vpr function have been widely investigated, the significance and the precise role(s) of Vpr *in vivo* remain unclear.

The main target of HIV-1 *in vivo* is CD4$^+$ T cells. Based on their function and phenotype, primary CD4$^+$ T cells are classified into three subsets: naive CD4$^+$ T cells (Tns), memory CD4$^+$ T cells (Tms), and regulatory CD4$^+$ T cells (Tregs). It is speculated that such phenotypic and functional differences among these subsets

Author Summary

HIV-1 encodes nine genes, five of which (*gag*, *pol*, *env*, *tat*, and *rev*) are essential for viral replication, and four, termed accessory genes (*vif*, *vpu*, *nef*, and *vpr*), appear to aid virus infection. Of the four accessory proteins, Vpr is the most enigmatic. It is well known that Vpr has the potential to cause G_2 cell cycle arrest and apoptosis *in vitro*. Moreover, it has been reported that Vpr-mediated G_2 arrest increases HIV-1 production *in vitro*. However, the role of Vpr in HIV-1 propagation *in vivo* remains unclear. Here, by using a humanized mouse model, we demonstrate that Vpr enhances CCR5-tropic but not CXCR4-tropic HIV-1 replication *in vivo* by exploiting Tregs during acute infection. In CCR5-tropic HIV-1-infected humanized mice, Vpr-dependent G_2 cell cycle arrest and apoptosis are predominantly observed in infected Tregs, and wild-type but not *vpr*-deficient HIV-1-infected mice displayed acute Treg depletion. This Vpr-dependent Treg depletion may lead to immune activation and provide a pool of activated/proliferating $CD4^+$ T cells, which supports subsequent HIV-1 expansion *in vivo*. This is the first report demonstrating the role of Vpr in HIV-1 infection *in vivo*.

closely associates with the infectivitiy, productivity, and replicativity of HIV-1 [6]. However, since cultured primary $CD4^+$ T cell subsets do not retain all of their *in vivo* attributes, the dynamics of each subset on HIV-1 infection are poorly understood.

Among the $CD4^+$ T cell subsets, Tregs constitute 5–10% of all $CD4^+$ T cells in human, monkey, and mouse species [7]. The potential and phenotype of Tregs are under the control of a transcription factor called forkhead box P3 (FOXP3), which is exclusively expressed in Tregs [8]. Tregs are more actively proliferating *in vivo* than the other $CD4^+$ T cell subsets [9–11]. It is well known that Tregs play a central role in the maintenance of self-tolerance and immune homeostasis [7]. In addition, it is implicated that Tregs are closely associated with immunopathological events such as autoimmune diseases [7] and infectious diseases [12–14]. In particular, there are lines of reports showing that HIV-1/SIV infection decreases Tregs in HIV-1-infected patients [15–17] and simian immunodeficiency virus (SIV)-infected macaque monkeys [18–20].

In this study, we infect a human hematopoietic stem cell (HSC)-transplanted humanized mouse model [21–25] with wild-type (WT) and *vpr*-deficient HIV-1 and investigate the fundamental role of Vpr in HIV-1 infection *in vivo*. Our findings suggest that Vpr plays a crucial role in accelerating CCR5-tropic (R5) but not CXCR4-tropic (X4) HIV-1 propagation during acute infection by utilizing $CCR5^+$ proliferating $CD4^+$ T cells including Tregs.

Results

Tregs are depleted during the acute phase of R5 HIV-1 infection

We first characterized the profile of human $CD4^+$ T cell subsets, including Tns, Tms, and Tregs, in human peripheral blood mononuclear cells (PBMCs) isolated from HIV-1-negative healthy donors and in the spleen of humanized mice [21–23]. As shown in Figure 1A, we detected 6.3±0.2% $FOXP3^+$ $CD4^+$ T cells in splenic human $CD4^+$ T cells of humanized mice, which was comparable to those in human peripheral $CD4^+$ T cells (5.4±0.6%; Figure 1B). Consistent with previous reports [26–29], we also confirmed that the phenotypes of Tregs including the expression levels of CD25, CD127, and cytotoxic T-lymphocyte

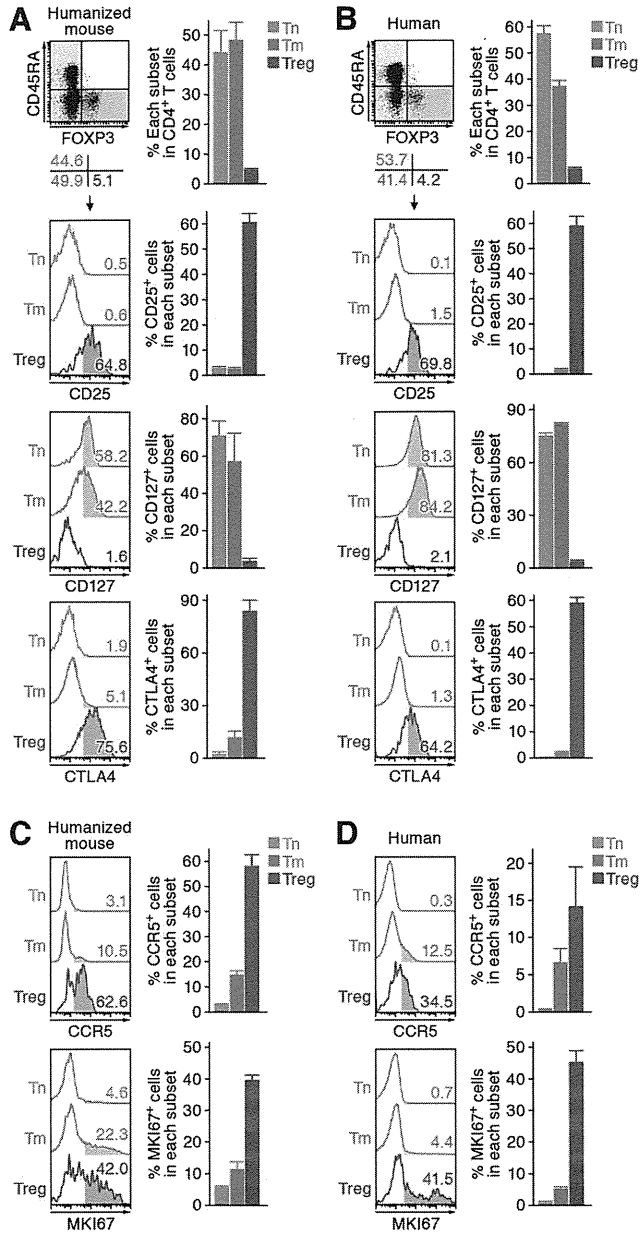

Figure 1. Comparison of the profile of $CD4^+$ T cell subsets between human and humanized mouse. Human $CD4^+$ T cells isolated from the spleen of humanized mice (A and C, n = 8) and the PB of HIV seronegative humans (B and D, n = 6) and were classified into Tn ($CD45^+$ $CD3^+$ $CD4^+$ $CD45RA^+$ $FOXP3^-$ cells), Tm ($CD45^+$ $CD3^+$ $CD4^+$ $CD45RA^-$ $FOXP3^-$ cells), and Treg ($CD45^+$ $CD3^+$ $CD4^+$ $CD45RA^-$ $FOXP3^+$ cells) by flow cytometry. Representative dot plots and histograms are shown on the left panels. The percentage of each subset in $CD4^+$ T cells (A and B, top) and the percentages of the cells positive for CD25, CD127, CTLA4, CCR5, and MKI67 in each subset are respectively shown on the right panels. In the left panels, the numbers under the dot plots (A and B, top) indicate the percentage of the cells in each quadrant, and the numbers in each histogram indicate the positivity. Data represent mean ± SEM.
doi:10.1371/journal.ppat.1003812.g001

associated protein 4 (CTLA4; also known as CD152) in humanized mice (Figure 1A) were similar to those in humans (Figure 1B). Since the suppressive function of the Tregs differentiated in humanized mouse models has been demonstrated previously [26–29], our results strongly suggest that the majority of

FOXP3$^+$ CD4$^+$ T cell population in our humanized mouse model is Tregs. Moreover, the expression level of CCR5, an HIV-1 coreceptor, was higher on Tregs than on Tms and Tns in both humans and humanized mice (Figure 1C and 1D). Furthermore, in line with previous studies reporting that Tregs actively proliferate *in vivo* [9–11], the percentage of the cells positive for MKI67 antigen identified by monoclonal antibody Ki-67 (MKI67; also known as Ki67) in Tregs of humans and humanized mice was significantly higher than those in Tms and Tns (Figure 1C and 1D). These results indicate that Tregs in humans and humanized mice are more actively cycling than Tns and Tms. Altogether, these results suggested that the profile and characteristics of CD4$^+$ T cell subsets in humanized mice mirror those in healthy humans.

To investigate the dynamics of each CD4$^+$ T cell subset after HIV-1 infection, 40 humanized mice were infected with a primary R5 HIV-1 isolate, strain JR-CSF [30]. As observed in HIV-1-infected individuals [15–17] and SIV-infected monkeys [18–20], we found that Tregs were preferentially and significantly decreased in the peripheral blood (PB) (Figure 2A and 2B) and the spleen (Figure 2C and 2D) of HIV-1-infected humanized mice until 21 days postinfection (dpi). However, because we have previously observed that surface CD4 molecules on HIV-1-infected cells in humanized mice are downregulated [21,23], we evaluated whether this was the case in Tregs. Results showed that Tregs were positive for surface CD4 (i.e., CD4$^-$ FOXP3$^+$ cells were absent) (Figure S1), indicating that the disappearance of Tregs during the acute phase of infection was not due to surface CD4 down-regulation, but rather to depletion by HIV-1 infection. Since CCR5 is highly expressed on Tregs (Figure 1C and 1D), we further assessed the level of CCR5$^+$ CD4$^+$ T cells in R5 HIV-1-infected humanized mice. As shown in Figure 2E, we observed zthat the percentage of CCR5$^+$ cells in the splenic CD4$^+$ T cells of R5 HIV-1-infected mice was significantly lower than that of mock-infected mice (Figure 2E). These findings suggest that R5 HIV-1 infection induces severe depletion of CCR5$^+$ CD4$^+$ T cells including Tregs during acute infection.

It is well known that Tregs have the potential to suppress immune activation *in vivo*, and that the depletion of Tregs induces aberrant immune activation [7]. To address this possibility in HIV-1-infected humanized mice, we assessed the immune activation status at 21 dpi by staining with CD38, an activation marker [31,32]. As shown in Figure 2F, the expression level of CD38 on memory CD8$^+$ T cells in the spleen of HIV-1-infected mice was significantly higher than that of mock-infected mice.

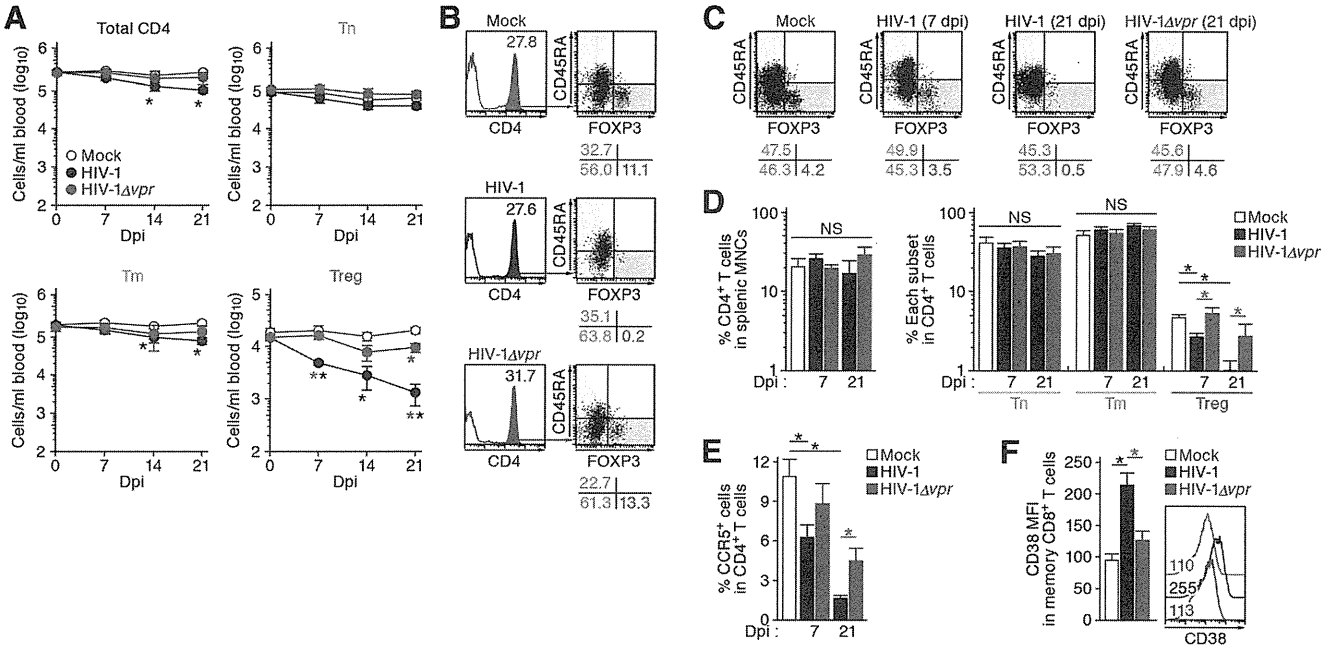

Figure 2. Dynamics of human CD4$^+$ T cell subsets in humanized mice infected with R5 WT and *vpr*-deficient HIV-1. (A and B) Longitudinal analyses of the dynamics of human CD4$^+$ T cell subsets in the PB of infected humanized mice. The numbers of total CD4$^+$ T cells (CD45$^+$ CD3$^+$ CD4$^+$ cells), Tns (CD45$^+$ CD3$^+$ CD4$^+$ CD45RA$^+$ FOXP3$^-$ cells), Tms (CD45$^+$ CD3$^+$ CD4$^+$ CD45RA$^-$ FOXP3$^-$ cells), and Tregs (CD45$^+$ CD3$^+$ CD4$^+$ CD45RA$^-$ FOXP3$^+$ cells) in the PB of R5 WT HIV-1-infected mice (n = 8), R5 *vpr*-deficient HIV-1-infected mice (n = 8), and mock-infected mice (n = 12) were routinely quantified by flow cytometry and hematocytometry. Summarized results (A) and representative dot plots at 21 dpi (B) are shown, respectively. In panel B, the numbers in the histogram indicate the percentage of CD4$^+$ cells in CD45$^+$ cells, and the numbers under the dot plots indicate the percentage of the cells in each quadrant. (C and D) Cytopathic effect of WT and *vpr*-deficient HIV-1 in the spleen of humanized mice. The percentages of total CD4$^+$ T cells, Tns, Tms, and Tregs in the splenic MNCs of WT HIV-1-infected mice (7 dpi, n = 19; 21 dpi, n = 8), *vpr*-deficient HIV-1-infected mice (7 dpi, n = 10; 21 dpi, n = 7), and mock-infected mice (n = 12) were routinely quantified by flow cytometry. Representative dot plots (C) and summarized results (D) are shown, respectively. In panel C, the numbers under the dot plots indicate the percentage of the cells in each quadrant. (E) The level of CCR5-expressing CD4$^+$ T cells in infected humanized mice. The percentage of CCR5$^+$ cells in the splenic CD4$^+$ T cells of WT HIV-1-infected mice (7 dpi, n = 8; 21 dpi, n = 6), *vpr*-deficient HIV-1-infected mice (7 dpi, n = 8; 21 dpi, n = 6), and mock-infected mice (n = 8) was analyzed by flow cytometry. (F) The level of immune activation in infected humanized mice. The MFI of CD38 in memory CD8$^+$ T cells (CD45$^+$ CD3$^+$ CD8$^+$ CD45RA$^-$ cells) in the spleen of WT HIV-1-infected mice (n = 5), *vpr*-deficient HIV-1-infected mice (n = 5), and mock-infected mice (n = 5) at 21 dpi was analyzed by flow cytometry. Representative histograms are shown on the right panel, and the numbers in the histogram indicate the MFI values. Statistical difference was determined by Welch's *t* test, and statistically significant differences ($P<0.05$) are shown as follows: mock versus WT HIV-1, black asterisk; mock versus HIV-1*Δvpr*, blue asterisk; and WT HIV-1 versus HIV-1*Δvpr*, red asterisk. NS, no statistical significance. Data represent mean ± SEM.

doi:10.1371/journal.ppat.1003812.g002

These results suggested that HIV-1 infection decreased Tregs in humanized mice and resulted in immune activation.

Vpr depletes Tregs and enhances HIV-1 propagation in a coreceptor-dependent manner

As described in Introduction section, Vpr is pleiotropic and is known to induce cell cycle arrest at the G_2 phase and apoptosis [1]. Since Tregs are highly proliferative *in vivo* (Figure 1), which is consistent with previous reports [9–11], we hypothesized that Tregs are highly susceptible to Vpr-mediated G_2 arrest. To test this hypothesis, 32 humanized mice were infected with R5 *vpr*-deficient HIV-1 (HIV-1*Δvpr*; strain JR-CSF) [33]. Although the infectivities of R5 WT HIV-1 and R5 HIV-1*Δvpr* were comparable *in vitro* (Figure S2), the level of viral load in the plasma of HIV-1*Δvpr*-infected mice at 4 and 7 dpi was significantly lower than that of WT HIV-1-infected mice (Figure 3A). These results suggested that HIV-1*Δvpr* is less replicative than WT HIV-1 during initial stage of infection in humanized mice. We also investigated the dynamics of $CD4^+$ T cells in HIV-1*Δvpr*-infected mice and found that the acute and severe depletion of Tregs after virus challenge was not observed in the PB (Figure 2A and 2B) and the spleen (Figure 2C and 2D). In addition, the level of $CCR5^+$ $CD4^+$ T cells in the spleen of HIV-1*Δvpr*-infected mice was significantly higher than that of WT HIV-1-infected mice (Figure 2E). Moreover, the immune activation, which was observed in WT HIV-1-infected mice, was not detected in HIV-1*Δvpr*-infected mice (Figure 2F). These findings suggested that Vpr enhances virus dissemination and induces Treg depletion leading to immune activation in humanized mice.

To address the association of Vpr with the rapid HIV-1 expansion *in vivo*, we next assessed the distribution of HIV-1-infected cells during acute infection (i.e., 7 dpi). As shown in Figure 3B, the percentage of the cells positive for p24, an HIV-1 antigen, in splenic $CD3^+$ $CD8^-$ cells of WT HIV-1-infected mice was comparable to that of HIV-1*Δvpr*-infected mice. We then examined the proportion of $p24^+$ cells in each $CD4^+$ T cell subset and found that Tregs were more positive for p24 than Tm and Tn in both WT HIV-1-infected and HIV-1*Δvpr*-infected mice (Figure 3C, left and right panels). In addition, we demonstrated that the percentage of $p24^+$ Tregs in WT HIV-1-infected mice was significantly higher than that in HIV-1*Δvpr*-infected mice (Figure 3C, left and right panels). Moreover, in WT HIV-1 but not in HIV-1*Δvpr*-infected mice, the mean fluorescent intensity (MFI) of p24, which reflects the expression level of viral proteins in infected cells, was significantly higher in Tregs than in Tns and Tms (Figure 3C, middle and right panels). Taken together, these results suggested that Tregs were highly susceptible to HIV-1 infection and produced large amounts of the virus with Vpr responsible for augmenting this production.

These findings raised the possibility that the preferential HIV-1 infection in Tregs was due to their high CCR5 expression (Figure 1C and 1D). To demonstrate this possibility, we assessed the expression level of CXCR4, another coreceptor for HIV-1, in each $CD4^+$ T cell subset. In both humans and humanized mice, we found that CXCR4 was broadly expressed in all $CD4^+$ T cell subsets and was highly expressed on Tns than Tms and Tregs (Figure 4A and 4B). Then, 13 humanized mice were infected with an X4 WT HIV-1 (strain NL4-3) [34], while 11 humanized mice were infected with an X4 HIV-1*Δvpr* (strain NL4-3) [2]. The infectivities of X4 WT HIV-1 and X4 HIV-1*Δvpr* were comparable *in vitro* (Figure S3). In contrast to the observations in R5 HIV-1-infected humanized mice (Figure 3A), the viral load of X4 WT HIV-1 and was comparable to that of X4 *vpr*-deficient HIV-1 (Figure 4C). In addition, the depletion of Tregs during the acute phase of infection, which was found in R5 HIV-1-infected mice (Figure 2A–2D), was not observed in the PB (Figure 4D) and the spleen (Figure 4E and 4F) of X4 WT HIV-1-infected mice. Furthermore, we did not observe the immune activation in X4 HIV-1-infected mice during acute infection (Figure 4G). Taken together, these findings strongly suggest that the preferential HIV-1 infection and the Treg depletion leading to immune activation during acute infection are dependent on the coreceptor usage of HIV-1.

Vpr induces a significant level of G_2 cell cycle arrest in infected Tregs

Extensive *in vitro* studies have reported that Vpr can cause cell cycle arrest at the G_2 phase [1]. To investigate the cell cycle condition of R5 HIV-1-infected cells in humanized mice at 7 dpi, cellular DNA content was quantified by Hoechst staining. Although the percentages of p24-negative cells at the G_2M phase in the spleen of WT HIV-1-infected and HIV-1*Δvpr*-infected cells were similar to those of mock-infected mice, a significant level of p24-positive cells at the G_2M phase in both WT HIV-1-infected and HIV-1*Δvpr*-infected mice were detected (Figure 5A). Moreover, we found that the percentage of $p24^+$

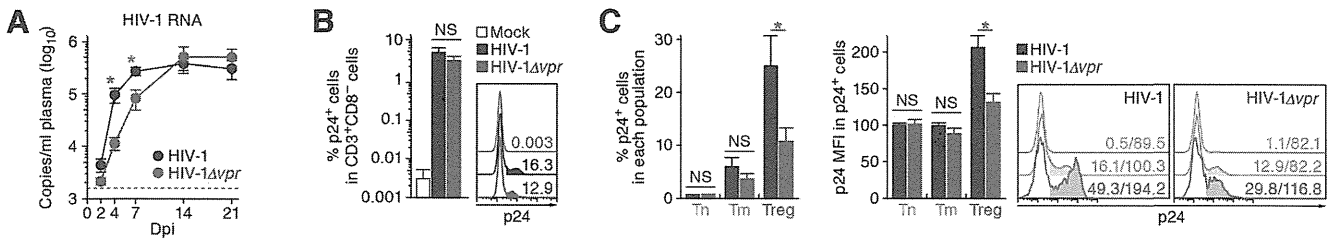

Figure 3. Dynamics of R5 WT and *vpr*-deficient HIV-1 infection in humanized mice. (A) Viral load in infected humanized mice. The amounts of viral RNA in the plasma of R5 WT HIV-1-infected mice (n = 30) and R5 *vpr*-deficient HIV-1-infected mice (n = 23) were routinely quantified. The horizontal broken line indicates the detection limit of the assay (1,600 copies/ml). (B and C) Infected cells in humanized mice. HIV-1-infected cells in the spleen of R5 WT HIV-1-infected mice (n = 19), R5 *vpr*-deficient HIV-1-infected mice (n = 10), and mock-infected mice (n = 10) at 7 dpi were analyzed by flow cytometry using an anti-HIV-1 p24 antibody. The percentages of $p24^+$ cells in $CD3^+$ $CD8^-$ cells (B) and in each $CD4^+$ T cell subset (C, left panel), and the MFI of p24 in $p24^+$ cells of each $CD4^+$ T cell subset (C, middle panel) are shown. Representative histograms are shown on the right panel. In panel B, the numbers in the histogram indicate the positivity. In panel C, the numbers in the histogram indicate the percentage of positive cells (left) and MFI values (right). Statistical difference was determined by Welch's *t* test, and statistically significant differences between WT HIV-1 versus HIV-1*Δvpr* ($P<0.05$) are shown with red asterisks. NS, no statistical significance. Data represent mean ± SEM.
doi:10.1371/journal.ppat.1003812.g003

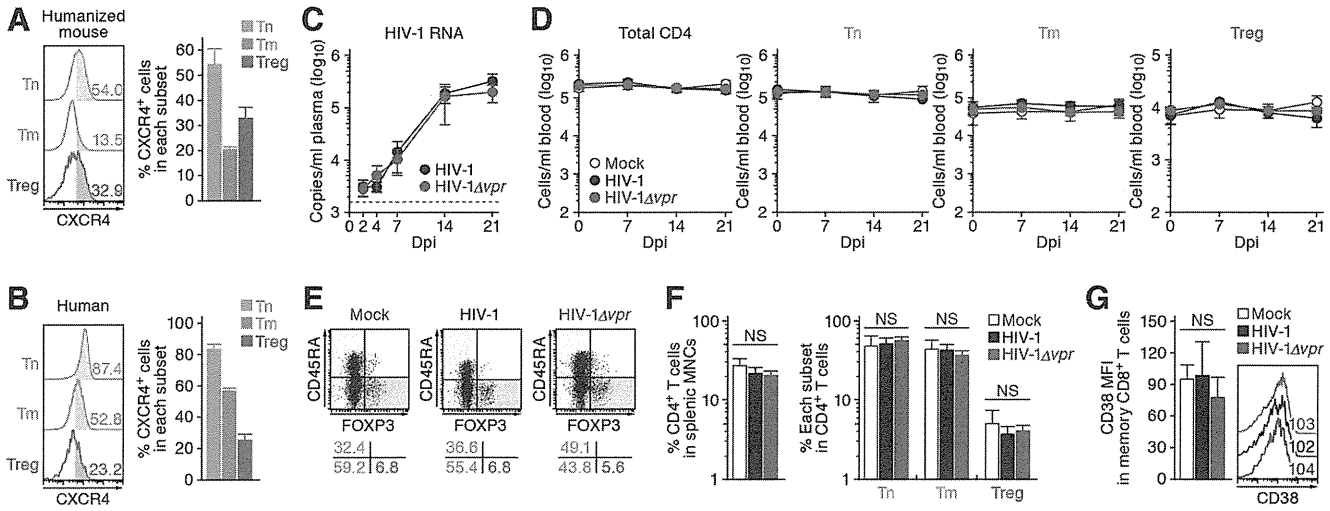

Figure 4. Dynamics of X4 WT and *vpr*-deficient HIV-1 infection in humanized mice. (A and B) CXCR4 expression on $CD4^+$ T cell subsets in human and humanized mouse. Human $CD4^+$ T cells isolated from the spleen of humanized mice (A, n = 8) and the PB of HIV seronegative humans (B, n = 6) were classified into Tn, Tm, and Treg as described in the legend of Figure 1. Representative dot plots and histograms are shown on the left, and the percentages of $CXCR4^+$ cells in each subset are shown on the right. In the left panels, the numbers in each histogram indicate the positivity. (C) Viral load in infected humanized mice. The amounts of viral RNA in the plasma of X4 WT HIV-1-infected mice (n = 13) and X4 *vpr*-deficient HIV-1-infected mice (n = 11) were routinely quantified. The horizontal broken line indicates the detection limit of the assay (1,600 copies/ml). (D) Longitudinal analyses of the dynamics of human $CD4^+$ T cell subsets in the PB of infected humanized mice. The numbers of total $CD4^+$ T cells, Tns, Tms, and Tregs in the PB of WT HIV-1-infected mice (n = 9), *vpr*-deficient HIV-1-infected mice (n = 9), and mock-infected mice (n = 8) were routinely quantified by flow cytometry and hematocytometry. (E and F) Cytopathic effect of WT and *vpr*-deficient HIV-1 in the spleen of humanized mice. The percentages of total $CD4^+$ T cells, Tns, Tms, and Tregs in the splenic MNCs of WT HIV-1-infected mice (n = 8), *vpr*-deficient HIV-1-infected mice (n = 8), and mock-infected mice (n = 8) at 21 dpi were routinely quantified by flow cytometry. Representative dot plots (E) and summarized results (F) are shown, respectively. In panel E, the numbers on the right of the dot plots indicate the percentage of the cells in each quadrant. (G) The level of immune activation in infected humanized mice. The MFI of CD38 in memory $CD8^+$ T cells in the spleen of WT HIV-1-infected mice (n = 5), *vpr*-deficient HIV-1-infected mice (n = 5), and mock-infected mice (n = 5) at 21 dpi was analyzed by flow cytometry. Representative histograms are shown on the right panel, and the numbers in the histogram indicate the MFI values. NS, no statistical significance. Data represent mean ± SEM.
doi:10.1371/journal.ppat.1003812.g004

cells at the G_2M phase in WT HIV-1-infected mice was significantly higher than that in HIV-1*Δvpr*-infected mice (Figure 5A), suggesting that Vpr expressed in infected cells induced G_2 cell cycle arrest *in vivo*.

We next analyzed the level of G_2 arrest in each $CD4^+$ T cell subset. Since $p24^+$ cells were faintly detected in the Tn subset (Figure 3C; 0.33±0.1% for WT HIV-1, 0.35±0.1% for HIV-1*Δvpr*), we focused on Tms and Tregs. In both subsets, the percentages of G_2M cells in $p24^-$ cells of WT HIV-1-infected and HIV-1*Δvpr*-infected mice were similar to those of mock-infected mice (Figure 5B). In contrast, we detected a significant level of $p24^+$ cells at the G_2M phase in Tms and Tregs (Figure 5B). Of note, the percentage of G_2M cells in $p24^+$ Tregs of WT HIV-1-infected mice reached a maximum of 37.1±2.8% and was significantly higher than that of HIV-1*Δvpr*-infected mice (Figure 5B). These results suggested that the level of Vpr-mediated G_2 arrest was the highest in HIV-1-infected Tregs.

Since it has been suggested that the G_2 arrest in HIV-1-infected cells results in the augmentation of virus production [3,35], we next focused on the relationship between the HIV-1 production potential and cell cycle condition in Tms and Tregs. Figure 5C illustrated that G_2M cells displayed higher percentages of p24-positive cells than G_0G_1 cells in both Tm and Treg. Surprisingly, 74.1±5.4% of Tregs at the G_2M phase in WT HIV-1-infected mice were positive for p24 (Figure 5C, left and right panels), and the p24 MFI in $p24^+$ Tregs at G_2M phase was highest (Figure 5C, middle and right panels). Taken together, these findings suggested that the majority of Tregs were infected with HIV-1 and arrested at the G_2 phase by Vpr, resulting in the augmentation of HIV-1 production during acute infection.

Vpr directly induces apoptosis in infected Tregs associated with G_2 cell cycle arrest

In addition to the augmentation of viral replication by Vpr, we also observed a severe depletion of Tregs in R5 WT HIV-1-infected humanized mice (Figure 2A–2D). It is known that Vpr can induce apoptosis through a caspase 3/8 (CASP3/8)-dependent pathway [1]. Therefore, we next analyzed the level of active CASP3, which is a direct inducer of apoptosis, in infected humanized mice. In the population of p24-negative cells, we found a significant increase of active $CASP3^+$ cells in WT HIV-1-infected mice (Figure 6A). Additionally, in both WT HIV-1-infected and HIV-1*Δvpr*-infected mice, the percentage of active CASP3 in $p24^+$ cells was significantly higher than that in $p24^-$ cells, yet the percentage of active CASP3 in $p24^+$ cells of WT HIV-1-infected cells was significantly higher than that of HIV-1*Δvpr*-infected mice (Figure 6A).

We then evaluated the magnitude of apoptosis in each $CD4^+$ T cell subset. As shown in Figure 6B, the percentage of active $CASP3^+$ cells in $p24^-$ Tms and Tregs of WT HIV-1-infected mice significantly increased when compared with those of mock-infected mice. On the other hand, the percentage of active $CASP3^+$ cells was significantly increased in $p24^+$ cells and was highest in $p24^+$ Tregs of WT HIV-1-infected mice (26.6±3.9%; Figure 6B), suggesting that Tregs are highly sensitive to Vpr-mediated apoptosis.

In addition to the apoptosis directly induced by Vpr, accumulating evidence has suggested a role for innate immune activation, including NK cells, in the $CD4^+$ T cell depletion after primary HIV-1 infection in individuals [36,37]. Also, it has been recently reported that Vpr upregulates the surface expression of some NK receptor ligands, such as UL16 binding protein 2

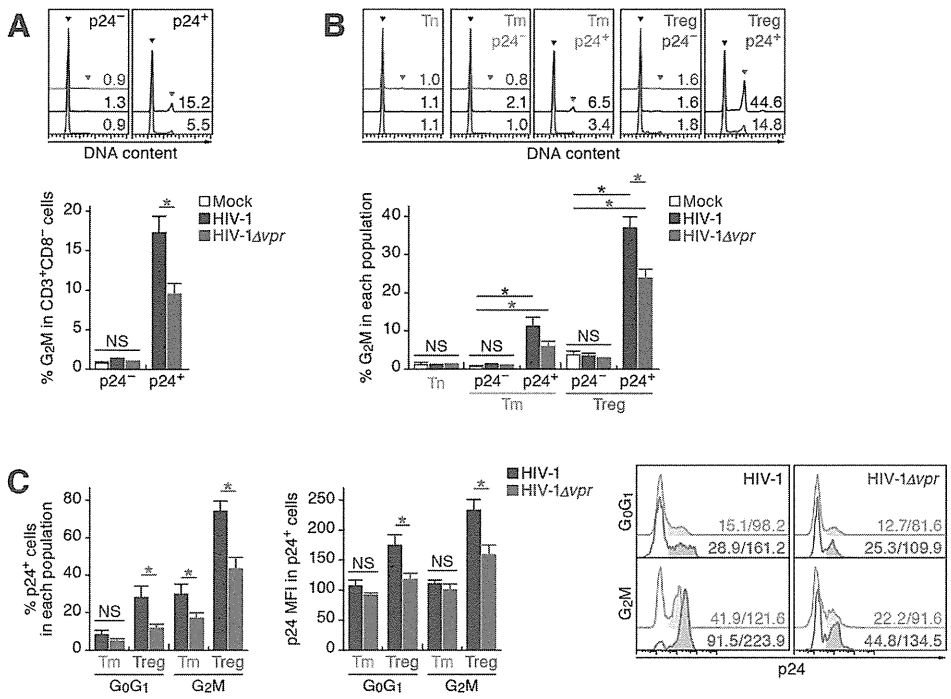

Figure 5. Effect of Vpr on G_2 cell cycle arrest in infected humanized mice. Splenic MNCs of WT HIV-1-infected mice (n = 12), *vpr*-deficient HIV-1-infected mice (n = 11), and mock-infected mice (n = 15) at 7 dpi were analyzed by flow cytometry using Hoechst33342 and an anti-HIV-1 p24 antibody. (A and B) The percentages of G_2M cells in $CD3^+$ $CD8^-$ cells (A) and in each population (B) are shown, respectively. Representative histograms are shown on the right panel. The black arrowhead indicates the peak of G_0G_1 cells, and the red arrowhead indicates the peak of G_2M cells. The numbers in the histogram indicate the percentage of G_2M cells in each population. (C) The percentage of $p24^+$ cells in each population (left) and the MFI of p24 in $p24^+$ cells of each population (middle). Representative histograms are respectively shown. The numbers in the histogram indicate the percentage of positive cells (left) and MFI values (right). Statistical differences were determined by Welch's *t* test, and statistically significant differences ($P<0.05$) are shown as follows: mock versus WT HIV-1, black asterisk; mock versus HIV-1*Δvpr*, blue asterisk; and WT HIV-1 versus HIV-1*Δvpr*, red asterisk. NS, no statistical significance. Data represent mean ± SEM.
doi:10.1371/journal.ppat.1003812.g005

(ULBP2), which leads to NK cell-dependent cell death [38,39]. These reports led to the hypothesis that Vpr upregulates the expression level of ULBP2 on HIV-1-infected Tregs and enhances NK cell-dependent cell death. To address this possibility, we assessed the expression level of ULBP2 in infected humanized mice. However, the expression level of ULBP2 on the surface of WT HIV-1-infected cells was comparable to those of HIV-1*Δvpr*-infected cells, uninfected cells, and the $CD4^+$ T cells in mock-infected mice (Figure S4). Taken together, these results suggested that the decrease of Tregs in R5 WT HIV-1-infected mice was not dependent on the NK cell-dependent cell death but due to Vpr expressed in infected cells.

In order to investigate the relationship between G_2 cell cycle arrest and apoptosis, both of which are mediated by Vpr, we performed p24 staining in combination with Hoechst and active CASP3 staining. In each $CD4^+$ T cell subset positive for p24, the percentage of active $CASP3^+$ cells at G_2M was significantly higher than that at the G_0G_1 phase (Figure 6C). Moreover, the percentage of active $CASP3^+$ cells was highest in $p24^+$ Tregs at G_2M in WT HIV-1-infected mice (35.9±5.4%; Figure 6C), strongly suggesting that Vpr-mediated apoptosis was most efficiently induced in infected Tregs arrested at the G_2 phase.

Treg depletion can trigger immune activation and augmented HIV-1 propagation *in vivo*

The aforementioned findings suggested that Vpr promotes R5 HIV-1 propagation during the acute phase of infection by exploiting proliferating $CCR5^+$ $CD4^+$ T cells including Tregs *in vivo*. In addition, Vpr is associated with the rapid decrease of Tregs, leading to immune activation. Since it is known that HIV-1 replicates more efficiently in activated $CD4^+$ T cells than non-activated $CD4^+$ T cells [40,41], our findings suggested that the immune activation induced by Vpr-mediated Treg depletion led to the augmented viral propagation *in vivo*. To address this possibility, denileukin diftitox (DD), which is known to specifically target and deplete Tregs, was intraperitoneally treated into humanized mice. As shown in Figure 7A and 7B, Tregs were specifically and significantly depleted by treatment with DD for 3 days, while the cell numbers of the other populations such as $CD45^+$ human white blood cells, total $CD4^+$ T cells, Tns, and Tms did not change significantly. We also found that the Treg depletion by DD induced immune activation and proliferation of splenic memory $CD8^+$ T cells (Figure 7C). Interestingly, the percentage of $MKI67^+$ cells in the Tms of DD-treated humanized mice was significantly higher than those in Tms and Tregs of untreated humanized mice (Figure 7D). In addition, the levels of CCR5 on Tms and Tns in DD-treated mice were significantly higher than that in untreated mice (Figure 7E), suggesting that the population size of proliferating $CCR5^+$ $CD4^+$ T cells in DD-treated humanized mice is greater than that in untreated humanized mice.

R5 WT and *vpr*-deficient HIV-1 (strain JR-CSF) were then inoculated into 13 DD-treated humanized mice, respectively. As shown in Figure 7F, the number of $CD4^+$ T cells, particularly Tms, in the PB of DD-treated uninfected mice gradually increased, while that those of DD-treated WT and *vpr*-deficient

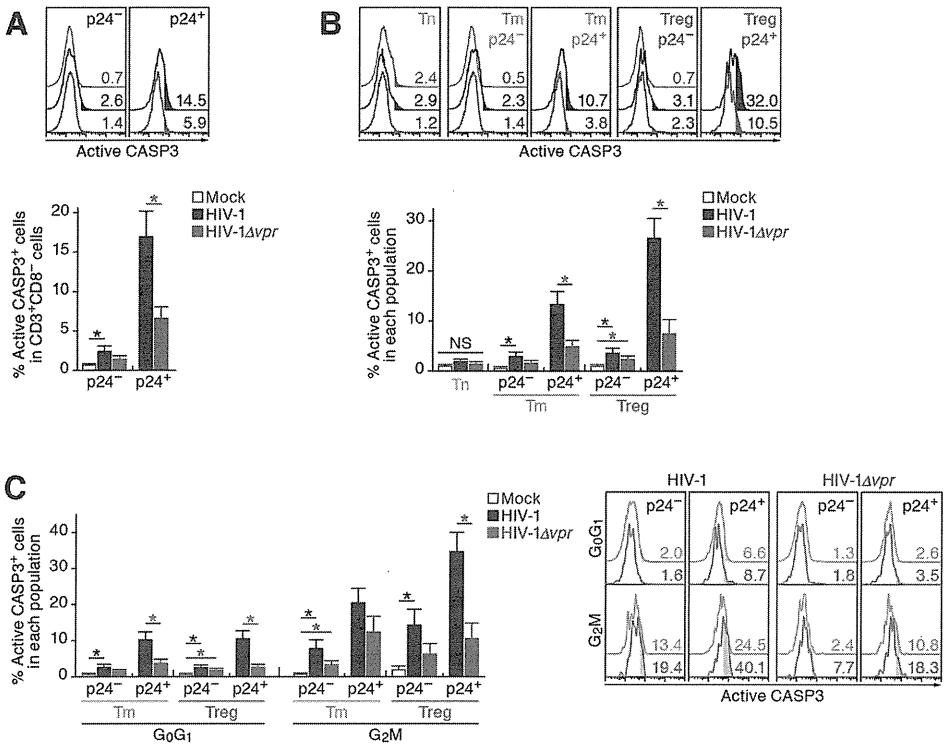

Figure 6. Effect of Vpr on apoptosis and its relevance in G_2 cell cycle arrest in infected humanized mice. Splenic MNCs of WT HIV-1-infected mice (n = 7), *vpr*-deficient HIV-1-infected mice (n = 7), and mock-infected mice (n = 9) at 7 dpi were analyzed by flow cytometry using anti-active CASP3 and anti-HIV-1 p24 antibodies without (A and B) or with (C) or Hoechst33342. (A and B) Effect of Vpr on apoptosis. The percentages of active $CASP3^+$ cells in $CD3^+$ $CD8^-$ cells (A) and in each population (B) are shown, respectively. Representative histograms are shown on the right panel. The numbers in the histogram indicate the percentage of active $CASP3^+$ cells in each population. (C) Relevance between G_2 arrest and apoptosis. The percentage of active $CASP3^+$ cells in each population is shown. Representative histograms are respectively shown. The numbers in the histogram indicate the percentage of active $CASP3^+$ cells in each population. Statistical differences were determined by Welch's *t* test, and statistically significant differences ($P<0.05$) are shown as follows: mock versus WT HIV-1, black asterisk; mock versus HIV-1*Δvpr*, blue asterisk; and WT HIV-1 versus HIV-1*Δvpr*, red asterisk. NS, no statistical significance. Data represent mean ± SEM.
doi:10.1371/journal.ppat.1003812.g006

HIV-1 infected mice severely decreased after 7 dpi. We also observed a gradual increase of memory $CD8^+$ T cells in the PB of DD-treated humanized mice regardless of HIV-1 infection (Figure S5). It was of particular importance that rapid and massive HIV-1 replication in DD-treated mice compared with untreated mice infected with either virus, and that the viral load in DD-treated WT HIV-1-infected mice was significantly higher than that in DD-treated HIV-1*Δvpr*-infected mice at 4 and 7 dpi (Figure 7G). Furthermore, the slope of virus growth in DD-treated WT HIV-1-infected mice was significantly higher than those of DD-treated HIV-1*Δvpr*-infected mice and untreated WT HIV-1-infected mice (Figure 7H). Taken together, these findings suggest that R5 HIV-1 massively propagates under an activated condition, and that Vpr enhances viral expansion in $CCR5^+$ proliferating $CD4^+$ T cell population.

Discussion

The fact that *vpr* is conserved in transmitted/founder viruses in infected individuals [42] may indicate its importance during the acute phase of HIV-1 propagation. However, even though there is abundant evidence of Vpr's roles in G_2 arrest and apoptosis *in vitro* [1,43,44], its impact on for HIV-1 replication *in vivo* remains unclear. In this study, we demonstrated that Vpr augments R5 HIV-1 propagation by exploiting proliferating $CCR5^+$ $CD4^+$ T cells including Tregs during acute infection. We also observed significant levels of Vpr-dependent G_2 arrest and apoptosis in R5 HIV-1-infected Tregs, which may result in the Treg depletion and subsequent immune activation. This is the first report to directly demonstrate that Vpr positively affects HIV-1 replication by taking advantage of Tregs *in vivo*.

A previous study has demonstrated that Tregs highly express CCR5, correlating with their high susceptibility to R5 HIV-1 *in vitro* [15]. Here, by using a humanized mouse model, we demonstrated that Tregs express higher level of CCR5 (Figure 1) and are highly susceptible to R5 HIV-1 infection *in vivo* (Figure 3). In addition, it is well known that HIV-1 replicates more efficiently in activated/proliferating cells than in non-activated cells [40,41]. Consistent with previous reports [9–11], we showed that Tregs are highly proliferative *in vivo* when compared with the other $CD4^+$ T cell subsets such as Tns and Tms (Figure 1). Therefore, it is reasonable to assume that R5 HIV-1 efficiently replicates in Tregs of humanized mice because of their higher CCR5 expression level and higher proliferating status. Moreover, in line with the previous observations that Vpr arrests the cell cycle of HIV-1-infected cells at G_2 phase where LTR-driven HIV-1 transcription is most active [3,35], we found that the MFI of p24, which reflects the expression level of viral proteins, in Tregs of WT HIV-1-infected mice was ~2-fold higher than that of HIV-1*Δvpr*-infected mice, while expression levels in Tns and Tms were comparable between WT and *vpr*-deficient HIV-1 (Figure 3C). Furthermore, we revealed that Vpr-dependent G_2

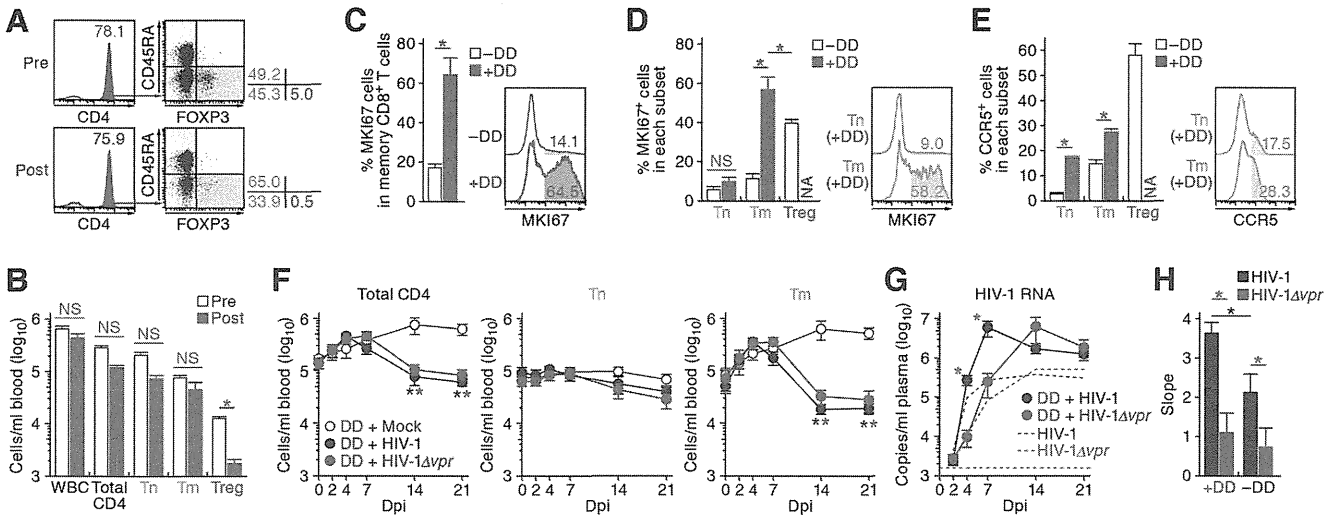

Figure 7. Augmentation of Vpr's effect and HIV-1 propagation by Treg depletion. (A to D) Evaluation of Treg depletion by treatment with DD. DD was administrated into humanized mice (n = 14) as described in Materials and Methods. (A and B) Specific depletion of Tregs by treatment with DD. The levels of human white blood cells (WBC; $CD45^+$ cells) and $CD4^+$ T cell subsets in PB of humanized mice before and after the DD treatment for 3 days were compared. Representatives (A) and the numbers of each human leukocytes in PB (B) are shown. In panel A, the numbers in the histogram indicate the percentage of $CD4^+$ cells in $CD45^+$ $CD3^+$ cells, and the numbers on the right of the dot plots indicate the percentage of the cells in each quadrant. (C and D) Immune activation by treatment with DD. The percentages of $MKI67^+$ cells in memory $CD8^+$ T cells (C) and in each $CD4^+$ T cell subset (D) in the spleen of humanized mice treated with (n = 5) or without (n = 8) DD for 7 days are shown, respectively. (E) Up-regulation of CCR5 expression by DD treatment. The percentage of $CCR5^+$ cells in each $CD4^+$ T cell subset in the spleen of humanized mice treated with (n = 5) or without (n = 8) DD for 7 days is shown. In panels C to E, the numbers in the histogram indicate positivity. (F to H) Dynamics of HIV-1 infection in DD-treated humanized mice. (F) The numbers of peripheral $CD4^+$ T cells, Tns, Tms, and Tregs (F) and the amounts of viral RNA in the plasma (G) of R5 WT HIV-1-infected DD-treated mice (n = 13), R5 *vpr*-deficient HIV-1-infected DD-treated mice (n = 13), and mock-infected DD-treated mice (n = 8) were routinely quantified as described in the legends of Figure 2A and 3A, respectively. In panel G, the broken black and blue lines indicate the averages of WT HIV-1-infected mice (n = 30) and *vpr*-deficient HIV-1-infected mice (n = 23) without DD treatment, which corresponds to the results shown in Figure 3A. The horizontal broken line indicates the detection limit of the assay (1,600 copies/ml). (H) Kinetics of viral expansion. The slopes of the amounts of viral RNA in the plasma of WT HIV-1-infected DD-treated mice (n = 13), *vpr*-deficient HIV-1-infected DD-treated mice (n = 13), WT HIV-1-infected mice (n = 30) and *vpr*-deficient HIV-1-infected mice (n = 23) until 7 dpi are shown. Statistical difference was determined by Welch's *t* test. In panels B to E, statistically significant differences ($P<0.05$) are indicated by red asterisks. In panels F and G, statistically significant differences ($P<0.05$) are shown as follows: mock versus WT HIV-1, black asterisk; mock versus HIV-1*Δvpr*, blue asterisk; and WT HIV-1 versus HIV-1*Δvpr*, red asterisk. In panel H, statistically significant differences ($P<0.05$) are shown as follows: with and without DD treatment, black asterisk; and WT HIV-1 versus HIV-1*Δvpr*, red asterisk. NS, no statistical significance. Data represent mean ± SEM. NA, not analyzed.
doi:10.1371/journal.ppat.1003812.g007

cell cycle arrest was efficiently occurred in infected Tregs (Figure 5B), and that both the percentage $p24^+$ cells and the p24 MFI was highest in WT HIV-1-infected Tregs at G_2 phase (Figure 5C). Taken together, these findings strongly suggest that Vpr promotes R5 HIV-1 replication during acute infection by increasing the viral production in Tregs.

In contrast to the findings in R5 HIV-1-infected humanized mouse model, we observed neither the acceleration of virus replication by Vpr during the acute phase of HIV-1 infection (Figure 4C), nor the Treg depletion (Figure 4D–4F), nor subsequent immune activation (Figure 4G) in X4 HIV-1-infected humanized mice. In Tregs, CCR5 is predominantly expressed (Figure 1C and 1D), whereas CXCR4 is broadly expressed in all $CD4^+$ T cell subsets (Figure 4A and 4B), which is consistent with previous findings [15,28]. Therefore, these results suggest that the Vpr-dependent augmentation of HIV-1 replication during acute infection is dependent on viral tropism and is restricted to R5 HIV-1. Regarding HIV-1 tropism, it is of particular importance that R5 HIV-1 is the major clinical isolates from patients, along with transmitted/founder viruses [42,45,46], while X4 HIV-1 occasionally emerges during the onset of AIDS [47,48]. Therefore, the findings in R5 HIV-1-infected humanized mice more properly reflect those in patients than those in X4 HIV-1-infected mice, and the role of Vpr in R5 HIV-1-infected humanized mice is physiologically more relevant.

The concept that Vpr augments R5 HIV-1 replication by utilizing proliferating $CCR5^+$ $CD4^+$ T cells is further supported by the DD treatment experiments (Figure 7): the human leukocytes including Tms in the mice treated with DD were highly proliferative and the Tms in DD-treated mice expressed higher level of CCR5. Moreover, R5 HIV-1 propagated more efficiently when compared with the untreated mice. Interestingly, it has been reported that Vpr enhances HIV-1 LTR-driven transcription in cycling $CD4^+$ T cells but not in non-cycling cells [3]. Taken together, these findings suggest that Vpr-dependent promotion of R5 HIV-1 production during acute infection is attributed to the target cell tropism of HIV-1 and the activated/proliferative status of the target cells.

There is a longstanding dogma that the immune activation caused by HIV-1/SIV infection closely associates with the disease progression [49]. Regarding the triggering of immune activation, previous studies have suggested that the immune activation in HIV-1-infected individuals and SIV-infected monkeys can be caused by (1) massive infection and loss of $CD4^+$ T cells [50,51]; (2) inflammatory cytokines [52,53]; and (3) microbial translocation from the luminal intestinal tract [54]. In this study, Treg depletion and immune activation were observed in R5 but not X4 HIV-1-infected humanized mice (Figure 2 and 4). These findings are consistent with previous observations in HIV-1-infected patients [15–17], SIV-infected monkeys [18–20], and a CCR5/CXCR4

dual-tropic HIV-1-infected humanized mouse model [28]. Particularly noteworthy is that *vpr*-deficient HIV-1-infected humanized mice showed neither Treg depletion nor immune activation. These findings raise a possibility that Vpr is associated with the induction of immune activation by depleting Tregs. Since the physiological role of Tregs *in vivo* is to suppress excessive immune activation [7], it is conceivable that Vpr-mediated Treg depletion can be one of the triggers for immune activation in HIV-1-infected individuals. However, the mechanism of the immune activation by HIV-1/SIV infection still remains unsolved for more than two decades of intense research, and there are lines of other possibilities such as the activation of dendritic cells/macrophages due to higher number of cell death [55–57] and the actual depletion of myeloid-derived suppressor cells [58,59] by direct or indirect virus infection. Although our results suggest that Vpr is associated with the acute Treg depletion and subsequent immune activation in R5 HIV-1-infected humanized mice, further investigations is necessary to elucidate the mechanisms of the immune activation by HIV-1/SIV infection.

In DD-treated humanized mice, we observed the activation/proliferation (Figure 7C) and the expansion (Figure S5) of memory $CD8^+$ T cells. As a previous report using R5 HIV-1-infected humanized mice showed that the depletion of $CD8^+$ T cells accelerates HIV-1 replication [60], these findings raise a possibility that the expanded memory $CD8^+$ T cells restrict HIV-1 replication in DD-treated humanized mice. However, the previous study [60] depleted $CD8^+$ T cells in R5 HIV-1-infected humanized mice during chronic infection (i.e, 5–7 weeks postinfection) and observed the increase of virus growth 2 weeks after $CD8^+$ T cell depletion. On the other hand, although the increase of memory $CD8^+$ T cells was observed in DD-treated humanized mice after 4 or 7 dpi (Figure S5), here we particularly focused on the dynamics of HIV-1 infection during the acute phase (i.e., until 7 dpi) and observed a sharp increase of HIV-1 replication in DD-treated mice prior to the expansion of memory $CD8^+$ T cells (Figure 7G). Moreover, the activation and expansion of $CD8^+$ T cells were detected in DD-treated humanized mice regardless of HIV-1 infection, strongly suggesting that this $CD8^+$ T cell expansion is not triggered by HIV-1 infection but by the DD-mediated Treg depletion. Furthermore, although the expansion of memory $CD8^+$ T cells during chronic infection has been observed in certain HIV-1-infected human HSC-transplanted humanized mouse models [61–63] including ours [25], it is controversial whether or not the human $CD8^+$ T cells differentiated in human HSC-transplanted humanized mouse models possess the potential to efficiently elicit acquired immune responses against pathogens including HIV-1 [64–66]. These findings suggest that the expanded $CD8^+$ T cells in DD-treated humanized mice have smaller effect on the virus growth during the acute phase of HIV-1 infection.

Soluble Vpr proteins are secreted from infected cells and can be detected in patient sera [67,68]. In p24-negative cells of WT HIV-1-infected mice, we found a significant level of apoptosis (Figure 6A and 6B), while G_2 arrest was not observed (Figure 5A and 5B). These results suggest that soluble Vpr can trigger apoptosis but not G_2 arrest in bystander cells. In fact, it was reported that the Vpr expressed in HIV-1-infected cells robustly induce both G_2 arrest and apoptosis, while soluble Vpr secreted from HIV-1-infected cells can induce apoptosis but not G_2 arrest [69]. However, in addition to WT HIV-1-infected cells, G_2 arrest was also partially observed in HIV-1*Δvpr*-infected cells (Figure 5A and 5B). In this regard, it has been reported that another accessory protein of HIV-1, Vif, is also able to cause G_2 arrest in a Vpr-independent manner [70–72], strongly suggesting that the G_2 arrest in HIV-1*Δvpr*-infected cells is induced by Vif. Although the significance of functional redundancy of Vpr and Vif for G_2 arrest remains unclear, further studies using humanized mice will reveal their impact.

In summary, we demonstrated for the first time that one of the major roles of Vpr in HIV-1 infection and pathogenesis is to enhance R5 HIV-1 propagation by exploiting proliferating $CCR5^+$ $CD4^+$ T cells including Tregs during acute infection, which can subsequently induce immune activation. Our findings suggest that the action of Vpr *in vivo* may provide HIV-1 with an optical condition to replicate and facilitate HIV-1 expansion *in vivo*.

Materials and Methods

Ethics statement

All procedures including animal studies were conducted following the guidelines for the Care and Use of Laboratory Animals of the Ministry of Education, Culture, Sports, Science and Technology, Japan. These studies were approved by the Institutional Animal Care and Use Committees (IACUC)/ethics committee of Kyoto University (protocol number D13–25). All protocols involving human subjects were reviewed and approved by the Kyoto University institutional review board. Informed written consent from human subjects was obtained in this study.

Humanized mice

NOD.Cg-*Prkdc*^{scid} *Il2rg*^{tm1Sug}/*Jic* (NOD/SCID *Il2rg*$^{-/-}$) mice [73] were obtained from the Central Institute for Experimental Animals (Kawasaki, Kanagawa, Japan). The mice were maintained under specific-pathogen-free conditions and were handled in accordance with the regulations of the IACUC/ethics committee of Kyoto University. Human $CD34^+$ HSCs were isolated from human fetal liver as described previously [74]. The humanized mouse (NOG-hCD34 mouse) was constructed as previously described [21–24]. Briefly, 164 newborn (aged 0 to 2 days) NOG mice from 38 litters were irradiated with X-ray (10 cGy per mouse) by an RX-650 X-ray cabinet system (Faxitron X-ray Corporation) and were then intrahepatically injected with the obtained human fetal liver-derived $CD34^+$ cells (7.5×10^4 to 25×10^4 cells). A list of the humanized mice used in this study is summarized in Table S1.

Virus preparation and infection

Virus solutions of R5 WT HIV-$1_{JR\text{-}CSF}$ [30], R5 *vpr*-deficient HIV-$1_{JR\text{-}CSF}$ [33], X4 WT HIV-$1_{NL4\text{-}3}$ [34], and X4 *vpr*-deficient HIV-$1_{NL4\text{-}3}$ [2] were prepared and titrated as previously described [23]. Virus solutions of 10^5 50% tissue culture infectious doses ($TCID_{50}$) were intraperitoneally inoculated into NOG-hCD34 mice. RPMI 1640 was used for mock infection.

HIV-1 RNA quantification, TZM-bl assay, and western blotting

The amount of HIV-1 RNA in plasma was quantified by Bio Medical Laboratories, Inc. TZM-bl assay and Western blotting were performed as previously described [22,23]. For Western blotting, mouse anti-Vpr antibody (clone 8D1) [68] and goat anti-p24 antiserum (ViroStat) were used.

PB collection and isolation of splenic mononuclear cells

PB and plasma were routinely collected as previously described [21–24]. Splenic human mononuclear cells (MNCs) were isolated as previously described [22–24].

Flow cytometry and hematocytometry

Flow cytometry was performed with FACSCanto (BD Biosceiences) as previously described [21–24]. Hematocytometry was performed with Celltac alpha MEK-6450 (Nihon Kohden Co) as previously described [23,24]. Briefly, 10 μl of the PB of humanized mice were used for hematometry, and the number of MNCs per microliter was measured. The antibodies used in flow cytometry analysis are listed in Table S2. For cell cycle analysis, cellular DNA was stained with Hoechst33342 (Invitrogen) as previously described [21], and DNA contents were analyzed by using ModFit LT software (Verify software house) according to the manufacture's protocol and as previously reported [72]. For the measurement of the level of apoptosis, anti-active CASP3 antibody conjugated with PE (BD Biosciences; Table S2) was used according to the manufacture's procedure.

Denileukin diftitox treatment for Treg depletion

Denileukin diftitox (DD; IL-2 conjugated with diphtheria toxin) were purchased from Ligand Pharma, Co. For Treg depletion in humanized mice, DD (400 μg/200 μl in PBS) were intraperitoneally treated once per day. For HIV-1 infection following DD treatment, the humanized mice treated with DD for 3 days were intraperitoneally inoculated with virus solutions of 10^5 $TCID_{50}$. RPMI 1640 was used as the mock infection. To maintain Treg depletion following virus inoculation, DD was intraperitoneally treated once per day.

Statistical analyses

Data were expressed as averages with SEMs. Significant differences ($P<0.05$) were determined by Welch's t test or Student's t test.

Accession numbers

SwissProt (http://www.uniprot.org/) or GenBank (http://www.ncbi.nlm.nih.gov/genbank) accession numbers for the proteins mentioned in the text are as follows: CD3 (P07766); CD4 (P01730); CD8 (NP_001759.3); CD25 (NP_000408.1); CD38 (P28907); CD45 (NP_002829.3); CD45RA (P08575); CD127 (P16871); CASP3 (P42574); CCR5 (P51681); CXCR4 (P61073); CTLA4 (P16410); FOXP3 (Q9BZS1); MKI67 (P46013); ULBP2 (Q9BZM5). These proteins were detected by flow cytometry using the antibodies listed in Table S2. The accession numbers from GenBank (http://www.ncbi.nlm.nih.gov/genbank) for the viruses mentioned in the text are as follows: HIV-1 strain JR-CSF (M38429.1); HIV-1 strain NL4-3 (M19921.2).

Supporting Information

Figure S1 Depletion of Treg by WT HIV-1 infection. The percentage of $FOXP3^+$ $CD4^-$ cells in splenic MNCs of WT HIV-1-infected mice (n = 5) and mock-infected mice (n = 5) at 21 dpi are shown. Representative dot plots are shown below. The numbers under the dot plots correspond to the percentage in each quadrant. NS, no statistical significance.
(TIF)

Figure S2 Infectivity of R5 WT and *vpr*-deficient HIV-1. R5 WT and *vpr*-deficient HIV-1 (strain JR-CSF) were prepared as described in Materials and Methods. (Top) Western blot analyses of the virions. (Bottom) TZM-bl assay. Prepared virus solutions were inoculated into TZM-bl indicator cells. The infectivities of these viruses were quantified as described in Materials and Methods and were normalized to the amount of p24. The assay was performed in triplicate. NS, no statistical significance.
(TIF)

Figure S3 Infectivity of X4 WT and *vpr*-deficient HIV-1. X4 WT and *vpr*-deficient HIV-1 (strain NL4-3) were prepared as described in Materials and Methods. (Top) Western blot analyses of the virions. (Bottom) TZM-bl assay. Prepared virus solutions were inoculated into TZM-bl indicator cells. The infectivities of these viruses were quantified as described in Materials and Methods and were normalized to the amount of p24. The assay was performed in triplicate. NS, no statistical significance.
(TIF)

Figure S4 No association of ULBP2 with the Treg depletion observed in WT HIV-1-infected mice. Splenic MNCs of WT HIV-1-infected mice (n = 7), *vpr*-deficient HIV-1-infected mice (n = 7), and mock-infected mice (n = 7) at 7 dpi were analyzed by flow cytometry using an anti-ULBP2 and an anti-HIV-1 p24 antibodies. The percentages of $ULBP2^+$ cells in $CD3^+$ $CD8^-$ cells (A) and in each population (B) are respectively shown. Representative histograms are shown on the right. The numbers in histogram indicate the percentage of active $CASP3^+$ cells in each population. Statistical difference was determined by Welch's t test. NS, no statistical significance.
(TIF)

Figure S5 Expansion of memory $CD8^+$ T cells in DD-treated humanized mice. The numbers of total $CD8^+$ T cells ($CD45^+$ $CD3^+$ $CD8^+$ cells), naïve $CD8^+$ T cells ($CD45^+$ $CD3^+$ $CD8^+$ $CD45RA^+$ cells), and memory $CD8^+$ T cells ($CD45^+$ $CD3^+$ $CD8^+$ $CD45RA^-$ cells) in the PB of R5 WT HIV-1-infected DD-treated mice (n = 13), R5 *vpr*-deficient HIV-1-infected DD-treated mice (n = 13), and mock-infected DD-treated mice (n = 8) were routinely quantified by flow cytometry and hematocytometry.
(TIF)

Table S1 Humanized mice used in this study. A full list of the 132 humanized mice used in this study.
(PDF)

Table S2 Antibodies used in flow cytometry analyses. A full list of antibodies used in this study.
(PDF)

Acknowledgments

We would like to thank Peter Gee (Institute for Virus Research, Kyoto University, Japan) and Keiko Okano (Research Administration Office, Kyoto University, Japan) for proofreading this manuscript, Yoshinori Fukazawa (Oregon Health and Science University, United States of America), Rob J. de Boer (Utrecht University, the Netherland), Shimon Sakaguchi, and Motonao Osaki (Institute for Medical Sciences, Kyoto University, Japan) for helpful suggestions and discussion, and Yuetsu Tanaka (University of the Ryukyus, Japan) and Akio Adachi (The University of Tokushima) for providing materials. We also thank all the members in the laboratory of Virus Pathogenesis, Institute for Virus Research, Kyoto University for lively discussion and Kotubu Misawa for the dedicated support.

Author Contributions

Conceived and designed the experiments: KS YK. Performed the experiments: KS NM YS. Analyzed the data: KS NM SI YS MM. Contributed reagents/materials/analysis tools: SI MM YI MI KA DSA. Wrote the paper: KS YK.

References

1. Andersen JL, Le Rouzic E, Planelles V (2008) HIV-1 Vpr: mechanisms of G2 arrest and apoptosis. Exp Mol Pathol 85: 2–10.
2. Ogawa K, Shibata R, Kiyomasu T, Higuchi I, Kishida Y, et al. (1989) Mutational analysis of the human immunodeficiency virus *vpr* open reading frame. J Virol 63: 4110–4114.
3. Gummuluru S, Emerman M (1999) Cell cycle- and Vpr-mediated regulation of human immunodeficiency virus type 1 expression in primary and transformed T-cell lines. J Virol 73: 5422–5430.
4. Eckstein DA, Sherman MP, Penn ML, Chin PS, De Noronha CM, et al. (2001) HIV-1 Vpr enhances viral burden by facilitating infection of tissue macrophages but not nondividing $CD4^+$ T cells. J Exp Med 194: 1407–1419.
5. Hoch J, Lang SM, Weeger M, Stahl-Hennig C, Coulibaly C, et al. (1995) *vpr* deletion mutant of simian immunodeficiency virus induces AIDS in rhesus monkeys. J Virol 69: 4807–4813.
6. Stevenson M (2003) HIV-1 pathogenesis. Nat Med 9: 853–860.
7. Sakaguchi S, Miyara M, Costantino CM, Hafler DA (2010) $FOXP3^+$ regulatory T cells in the human immune system. Nat Rev Immunol 10: 490–500.
8. Hori S, Nomura T, Sakaguchi S (2003) Control of regulatory T cell development by the transcription factor Foxp3. Science 299: 1057–1061.
9. Fisson S, Darrasse-Jeze G, Litvinova E, Septier F, Klatzmann D, et al. (2003) Continuous activation of autoreactive $CD4^+CD25^+$ regulatory T cells in the steady state. J Exp Med 198: 737–746.
10. Vukmanovic-Stejic M, Zhang Y, Cook JE, Fletcher JM, McQuaid A, et al. (2006) Human $CD4^+CD25^{hi}Foxp3^+$ regulatory T cells are derived by rapid turnover of memory populations in vivo. J Clin Invest 116: 2423–2433.
11. Miyara M, Yoshioka Y, Kitoh A, Shima T, Wing K, et al. (2009) Functional delineation and differentiation dynamics of human $CD4^+$ T cells expressing the FoxP3 transcription factor. Immunity 30: 899–911.
12. Dittmer U, He H, Messer RJ, Schimmer S, Olbrich AR, et al. (2004) Functional impairment of $CD8^+$ T cells by regulatory T cells during persistent retroviral infection. Immunity 20: 293–303.
13. Weiss L, Donkova-Petrini V, Caccavelli L, Balbo M, Carbonneil C, et al. (2004) Human immunodeficiency virus-driven expansion of $CD4^+CD25^+$ regulatory T cells, which suppress HIV-specific CD4 T-cell responses in HIV-infected patients. Blood 104: 3249–3256.
14. Holmes D, Jiang Q, Zhang L, Su L (2008) Foxp3 and Treg cells in HIV-1 infection and immuno-pathogenesis. Immunol Res 41: 248–266.
15. Oswald-Richter K, Grill SM, Shariat N, Leelawong M, Sundrud MS, et al. (2004) HIV infection of naturally occurring and genetically reprogrammed human regulatory T-cells. PLoS Biol 2: E198.
16. Apoil PA, Puissant B, Roubinet F, Abbal M, Massip P, et al. (2005) FOXP3 mRNA levels are decreased in peripheral blood $CD4^+$ lymphocytes from HIV-positive patients. J Acquir Immune Defic Syndr 39: 381–385.
17. Eggena MP, Barugahare B, Jones N, Okello M, Mutalya S, et al. (2005) Depletion of regulatory T cells in HIV infection is associated with immune activation. J Immunol 174: 4407–4414.
18. Pereira LE, Villinger F, Onlamoon N, Bryan P, Cardona A, et al. (2007) Simian immunodeficiency virus (SIV) infection influences the level and function of regulatory T cells in SIV-infected rhesus macaques but not SIV-infected sooty mangabeys. J Virol 81: 4445–4456.
19. Chase AJ, Yang HC, Zhang H, Blankson JN, Siliciano RF (2008) Preservation of $FoxP3^+$ regulatory T cells in the peripheral blood of human immunodeficiency virus type 1-infected elite suppressors correlates with low $CD4^+$ T-cell activation. J Virol 82: 8307–8315.
20. Favre D, Lederer S, Kanwar B, Ma ZM, Proll S, et al. (2009) Critical loss of the balance between Th17 and T regulatory cell populations in pathogenic SIV infection. PLoS Pathog 5: e1000295.
21. Nie C, Sato K, Misawa N, Kitayama H, Fujino H, et al. (2009) Selective infection of $CD4^+$ effector memory T lymphocytes leads to preferential depletion of memory T lymphocytes in R5 HIV-1-infected humanized NOD/SCID/IL-$2R\gamma^{null}$ mice. Virology 394: 64–72.
22. Sato K, Izumi T, Misawa N, Kobayashi T, Yamashita Y, et al. (2010) Remarkable lethal G-to-A mutations in *vif*-proficient HIV-1 provirus by individual APOBEC3 proteins in humanized mice. J Virol 84: 9546–9556.
23. Sato K, Misawa N, Fukuhara M, Iwami S, An DS, et al. (2012) Vpu augments the initial burst phase of HIV-1 propagation and downregulates BST2 and CD4 in humanized mice. J Virol 86: 5000–5013.
24. Sato K, Misawa N, Nie C, Satou Y, Iwakiri D, et al. (2011) A novel animal model of Epstein-Barr virus-associated hemophagocytic lymphohistiocytosis in humanized mice. Blood 117: 5663–5673.
25. Sato K, Nie C, Misawa N, Tanaka Y, Ito M, et al. (2010) Dynamics of memory and naive $CD8^+$ T lymphocytes in humanized NOD/SCID/IL-$2R\gamma^{null}$ mice infected with CCR5-tropic HIV-1. Vaccine 28 Suppl 2: B32–37.
26. Billerbeck E, Barry WT, Mu K, Dorner M, Rice CM, et al. (2011) Development of human $CD4^+FoxP3^+$ regulatory T cells in human stem cell factor-, granulocyte-macrophage colony-stimulating factor-, and interleukin-3-expressing NOD-SCID IL2Rγ^{null} humanized mice. Blood 117: 3076–3086.
27. Duan K, Zhang B, Zhang W, Zhao Y, Qu Y, et al. (2011) Efficient peripheral construction of functional human regulatory $CD4^+CD25^{high}Foxp3^+$ T cells in NOD/SCID mice grafted with fetal human thymus/liver tissues and $CD34^+$ cells. Transpl Immunol 25: 173–179.
28. Jiang Q, Zhang L, Wang R, Jeffrey J, Washburn ML, et al. (2008) $FoxP3^+CD4^+$ regulatory T cells play an important role in acute HIV-1 infection in humanized $Rag2^{-/-}\gamma C^{-/-}$ mice in vivo. Blood 112: 2858–2868.
29. Onoe T, Kalscheuer H, Danzl N, Chittenden M, Zhao G, et al. (2011) Human natural regulatory T cell development, suppressive function, and postthymic maturation in a humanized mouse model. J Immunol 187: 3895–3903.
30. Koyanagi Y, Miles S, Mitsuyasu RT, Merrill JE, Vinters HV, et al. (1987) Dual infection of the central nervous system by AIDS viruses with distinct cellular tropisms. Science 236: 819–822.
31. Bofill M, Mocroft A, Lipman M, Medina E, Borthwick NJ, et al. (1996) Increased numbers of primed activated $CD8^+CD38^+CD45RO^+$ T cells predict the decline of $CD4^+$ T cells in HIV-1-infected patients. AIDS 10: 827–834.
32. Benito JM, Lopez M, Lozano S, Martinez P, Gonzalez-Lahoz J, et al. (2004) CD38 expression on CD8 T lymphocytes as a marker of residual virus replication in chronically HIV-infected patients receiving antiretroviral therapy. AIDS Res Hum Retroviruses 20: 227–233.
33. Kawano Y, Tanaka Y, Misawa N, Tanaka R, Kira JI, et al. (1997) Mutational analysis of human immunodeficiency virus type 1 (HIV-1) accessory genes: requirement of a site in the nef gene for HIV-1 replication in activated $CD4^+$ T cells *in vitro* and *in vivo*. J Virol 71: 8456–8466.
34. Adachi A, Gendelman HE, Koenig S, Folks T, Willey R, et al. (1986) Production of acquired immunodeficiency syndrome-associated retrovirus in human and nonhuman cells transfected with an infectious molecular clone. J Virol 59: 284–291.
35. Goh WC, Rogel ME, Kinsey CM, Michael SF, Fultz PN, et al. (1998) HIV-1 Vpr increases viral expression by manipulation of the cell cycle: a mechanism for selection of Vpr *in vivo*. Nat Med 4: 65–71.
36. Vieillard V, Strominger JL, Debre P (2005) NK cytotoxicity against $CD4^+$ T cells during HIV-1 infection: a gp41 peptide induces the expression of an NKp44 ligand. Proc Natl Acad Sci U S A 102: 10981–10986.
37. Chang JJ, Altfeld M (2010) Innate immune activation in primary HIV-1 infection. J Infect Dis 202 Suppl 2: S297–301.
38. Ward J, Davis Z, DeHart J, Zimmerman E, Bosque A, et al. (2009) HIV-1 Vpr triggers natural killer cell-mediated lysis of infected cells through activation of the ATR-mediated DNA damage response. PLoS Pathog 5: e1000613.
39. Richard J, Sindhu S, Pham TN, Belzile JP, Cohen EA (2010) HIV-1 Vpr up-regulates expression of ligands for the activating NKG2D receptor and promotes NK cell-mediated killing. Blood 115: 1354–1363.
40. Stevenson M, Stanwick TL, Dempsey MP, Lamonica CA (1990) HIV-1 replication is controlled at the level of T cell activation and proviral integration. EMBO J 9: 1551–1560.
41. Zack JA, Arrigo SJ, Weitsman SR, Go AS, Haislip A, et al. (1990) HIV-1 entry into quiescent primary lymphocytes: molecular analysis reveals a labile, latent viral structure. Cell 61: 213–222.
42. Salazar-Gonzalez JF, Salazar MG, Keele BF, Learn GH, Giorgi EE, et al. (2009) Genetic identity, biological phenotype, and evolutionary pathways of transmitted/founder viruses in acute and early HIV-1 infection. J Exp Med 206: 1273–1289.
43. Jowett JB, Planelles V, Poon B, Shah NP, Chen ML, et al. (1995) The human immunodeficiency virus type 1 vpr gene arrests infected T cells in the G2+M phase of the cell cycle. J Virol 69: 6304–6313.
44. Rogel ME, Wu LI, Emerman M (1995) The human immunodeficiency virus type 1 *vpr* gene prevents cell proliferation during chronic infection. J Virol 69: 882–888.
45. Parrish NF, Wilen CB, Banks LB, Iyer SS, Pfaff JM, et al. (2012) Transmitted/founder and chronic subtype C HIV-1 use CD4 and CCR5 receptors with equal efficiency and are not inhibited by blocking the integrin $\alpha4\beta7$. PLoS Pathog 8: e1002686.
46. Keele BF, Giorgi EE, Salazar-Gonzalez JF, Decker JM, Pham KT, et al. (2008) Identification and characterization of transmitted and early founder virus envelopes in primary HIV-1 infection. Proc Natl Acad Sci U S A 105: 7552–7557.
47. Koot M, van 't Wout AB, Kootstra NA, de Goede RE, Tersmette M, et al. (1996) Relation between changes in cellular load, evolution of viral phenotype, and the clonal composition of virus populations in the course of human immunodeficiency virus type 1 infection. J Infect Dis 173: 349–354.
48. Mosier DE (2009) How HIV changes its tropism: evolution and adaptation? Curr Opin HIV AIDS 4: 125–130.
49. Brenchley JM, Silvestri G, Douek DC (2010) Nonprogressive and progressive primate immunodeficiency lentivirus infections. Immunity 32: 737–742.
50. Brenchley JM, Schacker TW, Ruff LE, Price DA, Taylor JH, et al. (2004) $CD4^+$ T cell depletion during all stages of HIV disease occurs predominantly in the gastrointestinal tract. J Exp Med 200: 749–759.
51. Veazey RS, DeMaria M, Chalifoux LV, Shvetz DE, Pauley DR, et al. (1998) Gastrointestinal tract as a major site of $CD4^+$ T cell depletion and viral replication in SIV infection. Science 280: 427–431.
52. Giavedoni LD, Velasquillo MC, Parodi LM, Hubbard GB, Hodara VL (2000) Cytokine expression, natural killer cell activation, and phenotypic changes in lymphoid cells from rhesus macaques during acute infection with pathogenic simian immunodeficiency virus. J Virol 74: 1648–1657.